Viscous radiation driven disks in fast rotating massive stars

ABIGALI RODRÍGUEZ JIMÉNEZ

Supervisor: Michel Curé

Co-supervisor: Ignacio Araya

Instituto de Física y Astronomía

Facultad de Ciencias

Universidad de Valparaíso

Magíster en Astrofísica

August 2022

Valparaíso, Chile.

⋆ ⋆ ⋆ Come my girl, let's walk together through the sky ⋆ ⋆ ⋆

This work is dedicated to all the people who have been part of my cosmic journey

⋆ ⋆ ⋆ Ven mi niña, caminemos juntos por el firmamento ⋆ ⋆ ⋆

Trabajo dedicado a todas las personas que han sido parte de mi travesía cósmica

This thesis is solely my own composition,
except where specifically indicated in the text.

Total or partial reproduction, for scientific or academic purposes,
is authorised including a bibliographic reference to this documment.

Abigali Rodríguez Jiménez
August 2022
Valparaíso, Chile

Acknowledgements

I want to thank the University of Valparaíso for financing my stay in the Master's Program in Astrophysics at its Institute of Physics and Astronomy (IFA-UV). To my thesis supervisor, Prof. Dr. Michel Curé, both for his hospitality and teachings. To my co-supervisor, Prof. Dr. Ignacio Araya, for his teachings and contributions in the preparation of this thesis. To all the members of the Massive Stars Group for sharing their knowledge about stellar winds in massive stars and for teaching me new computational skills. I also want to thank to all the professors and colleagues of the IFA-UV who supported me inside and outside the academic field. Additionally, my supervisors and I thank the FONDECYT projects 1190485 and 11190147, as well as the POEMS project.

In the personal context I want to thank my mom, Lizbeth Jiménez Velázquez, because without her I would not be where I am now. Thank you for loving me so much and for always giving me your unconditional support. To my brother, Aarón, for caring about me and giving me life advices. To my dad, Juan Luis Rodríguez Noria, whose love, teachings and memories are beautiful constellations that I see in the sky when I feel lost. To my boyfriend, Alan, whose love and patience greatly influenced the development of this thesis. To Alan's parents, "Uncle" Carlos Carrero and "Aunt" Maggy Valencia, to whom I am indebted for all their care, understanding and affection. I thank my aunt Betina and my uncle Felix, who supported me in one of the most difficult moments that I went through when I started my master's degree. To my best friend, Ana, because I continue to count on her both in the best moments of my life and in the most gray and complicated days. To my friend Pablo, who has always extended his hand to help me. To Dr. Klaus-Peter Schröder and to Ilse for their friendship and for continuing to support me in my training as an astrophysicist. To the rest of my family and friends for keeping me in their prayers and in their hearts.

Abstract

Previous studies of equatorial winds from high rotating massive stars, considered angular momentum conservation, have found a dependency between stellar rotation rate (Ω) and a new type of solution: the Ω-slow solution (for $\Omega \gtrsim 0.75$), characterized by winds with low terminal velocities and high densities. It is believed that this type of solution could explain the low terminal velocities from the observational results of classical Be stars, which are the fastest rotating stars among non-degenerate stars.

From the study of wind solutions of fast rotating main sequence B-type stars, considering models with winds rotating in a quasi-Keplerian way (without conservation of angular momentum), the main objective of this work is to obtain a wind velocity profile that reproduce the low terminal velocities of classical Be stars. For this purpose, we introduced a parameter that mimics viscosity ($\gamma_{\rm vis}$) into the 1D nonlinear stationary differential equation of radiation driven winds (based on the m-CAK model) and we solved it using the hydrodynamic code HYDWIND.

Compared to the models where the wind rotates conserving angular momentum ($\gamma_{\rm vis} = 1.0$), the models of B2 V and B2.5 V stars studied in this work, where their winds rotate in a quasi-Keplerian way ($0.5 < \gamma_{vis} < 1.0$), present Ω-slow solutions with low terminal velocities. When $\gamma_{vis} \longrightarrow 0.5$, the lower the terminal velocity. On the other hand, using eight different main sequence B-type stars with a given interval of Ωs, we studied the influence of $\gamma_{\rm vis}$ in the region where standard m-CAK solutions and Ω-slow solutions can co-exist, called the co-existence region. Our results show that when the wind rotates in a quasi-Keplerian way, the interval of values of Ω, corresponding to the co-existence region, is shifted to higher values of Ω.

Contents

CHAPTER 1

Introduction

Stars, the fundamental unit of the luminous bodies that cover the night sky, can be classified in different ways according to their physical properties, for example, according to their masses. In the case of massive stars ($M_* > 8M_\odot$), these are very hot and very bright stellar objects sub-classified depending of their temperature as O, B and early A spectral type. Additionally, these stars contribute to the evolution of the interstellar medium due to their high mass loss throughout their lives.

Although during the main sequence massive stars are similar to other stars (they fuse hydrogen in their cores to produce helium), massive stars evolve faster than other stars. After the main sequence, throughout their evolution, massive stars generate the heaviest elements that can be produced from stellar thermonuclear fusions: electrons in the core of massive stars, and in some cases in layers closer to the core, degenerate every time the core fuel is depleted, to the point where the degeneration pressure cannot continue to counter the gravity. This is when from the combination of electrons and protons, electron-neutrinos and neutrons begin to be produced. In this way, when neutrons in the core and electrons in layers close to the core degenerate, the fusion of more elements will continue until the degeneracy pressure of these particles can no longer counteract the gravity of the star. As a consequence, these stars explode as supernovae upon reaching their last evolutionary phase and depending on how massive they are, their remnants can be neutron stars or stellar black holes.

In this work our object of study are classical Be stars, which are classified as massive stars. Classical Be stars, also mentioned only as Be stars, are the speediest rotators among non-degenerate stars. This particular characteristic could be probably the responsible of the presence of an outflowing gaseous disk in their equatorial planes (for an illustrative example see figure 1.1), called decretion-disk.

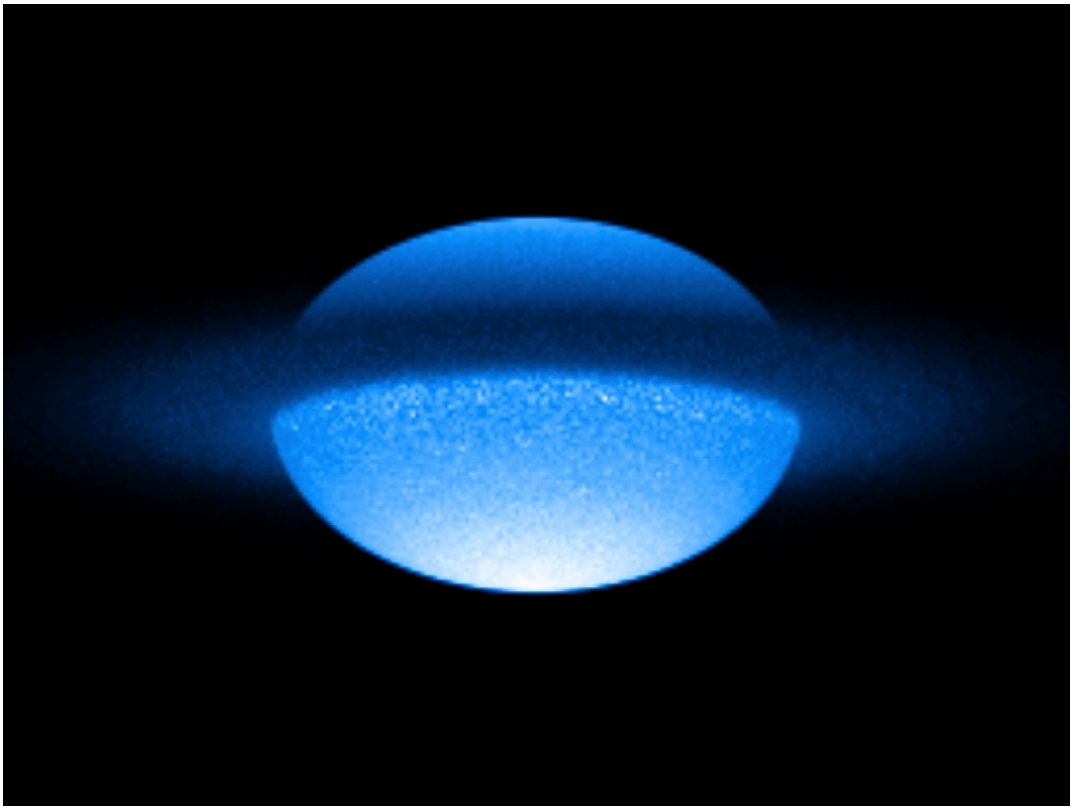

Figure 1.1: Illustrative example of a Be star with its gaseous disk. Credits: Daniel Moser Faes.

By definition, classical Be stars are massive fast rotating non-supergiant stars that present or have presented in their spectra one or more Balmer lines in emission at some time (Rivinius et al. 2013). The letter "e" in Be is a nomenclature used to referring the emission lines formed by the re-processing stellar ultraviolet light in the gaseous disk of Be stars. Particularly, the shape of these spectral lines depends on the inclination of the rotation axis with respect to the line of sight: because disk's rotation, while looking closer to the equator, a double-peaked emission is strongly evident.

Because decretion-disks are made of material ejected from the central star, this

type of disks can be modeled as a rotating radiation driven winds, based on the called m-CAK theory (Castor et al. 1975, Friend & Abbott 1986, Pauldrach et al. 1986). However, at present, the mechanism of formation and/or dissipation of these disks remains unknown and the relationship of the high rotation with that mechanism is still being studied (Araya et al. 2018).

Others non-degenerate fast rotators are Bn stars, which show broadened absorption lines, characteristics of fast rotations in stellar spectra, but do not show any lines of hydrogen in emission. It is believed that these type of stars could be of the same class of Be stars, but this has not yet been confirmed (Cochetti et al. 2020).

1.1 Winds from massive stars

Massive stars present what are known as stellar winds, that is, an outflow of particles expelled into outer space. In technical terms, the winds of massive stars are known as line driven winds or radiation driven winds, because they are driven by the momentum transfer of radiation from the star's photosphere to the gas through the absorption and reemission of photons. This winds enrich the interstellar medium, influencing their chemical composition. In general, almost all kinds of stars exhibit stellar winds at some point in their lives, however, due to their high luminosity, massive stars exhibit strong winds throughout their lives.

1.1.1 Historical studies

As Lamers & Cassinelli (1999) mention in their book, the history of the stellar winds begins in the year 1572 when Tycho Brahe observed a new type of star: a nova. This event gave rise to a universe where the stars are not perfect, but on the contrary, they are objects that do not always maintain a balance. Later in the 19th century, spectral observations of the variable star P-Cygni were made. Among the results were found spectral lines with a shape similar to the shape of the spectral lines detected in novae (this type of shape is now known as P-Cygni profile; see subsection 1.1.2), which led to the astronomers to think that both objects were experiencing the same phenomenon.

Already in the twentieth century theories were developed about the solar wind and about the structure of the atmospheres of the Sun and stars. As part of these

studies, Eugene Parker (Parker 1960) called stellar winds to the material that stars expelled into outer space. On the other hand, with the launch of telescopes on board of satellites, P-Cygni profiles were observed in ultraviolet range in the 1960s, corresponding to outflows in hot stars (Morton 1967, Snow & Morton 1976). In this way, the spectral information was expanded to shorter wavelengths.

Although the theory of stellar winds in massive stars had its beginnings with studies of gas dynamics in solar winds (Parker 1958), it was not until inconsistencies were found between the effective temperature needed to obtain the observed terminal velocities and the temperature at which the ions present in the photosphere are destroyed, which had to be considered a new mechanism for driving winds in massive stars. Lucy & Solomon (1970) considered this mechanism to be related to the absorption of resonance lines and Castor et al. (1975) refined the theory by considering the Sobolev approximation and building an analytical wind model parameterizing the contribution of the spectral lines to the radiative acceleration (CAK theory). This parameterization is given by a power law distribution, such that $M(t) = k\,t^{-\alpha}$; where $M(t)$ is the force multiplier function and t is the optical depth parameter. k and α were known as force multiplier parameters.

From 1980 to the present, instabilities and non-spherical effects in stellar winds have been studied. For example, Friend & Abbott (1986) and Pauldrach et al. (1986) implemented a modification to the CAK theory, where the star was considered as a finite disk and not as a point object (m-CAK theory). Another examples are the studies focus in the consequences of stellar rotation in the theory of winds, based on the observed broadened photospheric lines presented in some massive stars. It is believed that one of the effects of the rapid rotation in stars with radiative driven winds are outflowing disks or decretion-disks, which are equatorial material moving outwards from a rotating stellar photosphere. To explain the formation of this type of disks Lamers & Pauldrach (1991) developed the rotation induced bi-stability (RIB) model and Bjorkman & Cassinelli (1993) developed the wind compressed disk (WCD) model. However, RIB and WCD models were discarded by Cranmer & Owocki (1995).

To reproduce the lower terminal velocities from the observational results of Be stars (see for example Poeckert & Marlborough 1978, Stee et al. 1995; Chesneau et al. 2005), de Araujo (1995) added an empirical parameter, mimicking viscosity,

to the 1D stationary equation of motion in the equatorial plane of the standard theory. His results, considering only the standard m-CAK solutions (hereafter fast solutions) with winds rotating in a Keplerian way, fitted the terminal velocities from the observational results with values of $\alpha \approx 0.05 - 0.1$ and $k \geq 0.3$. However, when α was small ($\alpha < 0.2$) mass loss rates from the observational results required quite large values of k. On the other hand, Curé (2004) theoretically studied rotation in rapidly rotating stars and discovered a new family of solutions to the 1D stationary equation of motion in the equatorial plane for radiation driven winds with rotation velocities higher than $\sim$ 75% of the critical rotation speed, the so-called Ω-slow solutions, characterized by a wind with lower terminal velocities and higher densities than those possessed by the fast solutions. In this study the hydrodynamical code called HYDWIND was developed to solve the 1D hydrodynamic equation.

Araya et al. (2018) studied a switching process of fast and Ω-slow solutions, a process that is believed could trigger the formation and/or dissipation of an outflowing equatorial disk in stars with sub-critical rotation. To obtain the solutions to the 1D stationary radial equation of motion in the equatorial plane they used HYDWIND. Furthermore, they studied the stability of those solutions with the time-dependent hydrodynamical code ZEUS-3D (Clarke 1996). From this work was corroborated the absence of stationary solutions for some particular values of δ (Venero et al. 2016) and was confirmed that time-dependent solutions are very sensitive to the initial trial solution.

1.1.2 Spectral lines due to stellar winds

The spectral lines of the winds are formed mainly by two physical mechanisms: line-scattering and emission by recombination. On the one hand, line-scattering is a process that occurs when a photon from the stellar photosphere, which was absorbed by an atom at a certain transition, changes direction (scatters) when the excited electron returns to its initial state. A particular case of this mechanism is when the transition line is from the ground state. In that case, the line formed is named the resonance line and the process is renamed the resonance scattering. This last mechanism gives rise to the emissions of the P-Cygni profile (see figure 1.2). On the other hand, recombination emission is a process where electrons that are free collide with ions and recombine at an excited energy level, causing photons to be released upon de-excitation. In massive

stars the temperature is so high that even their atmospheres are made up of ions. For this reason, in hot star winds, the emissions on the Hα line and on the infrared lines come from this mechanism (Lamers & Cassinelli 1999).

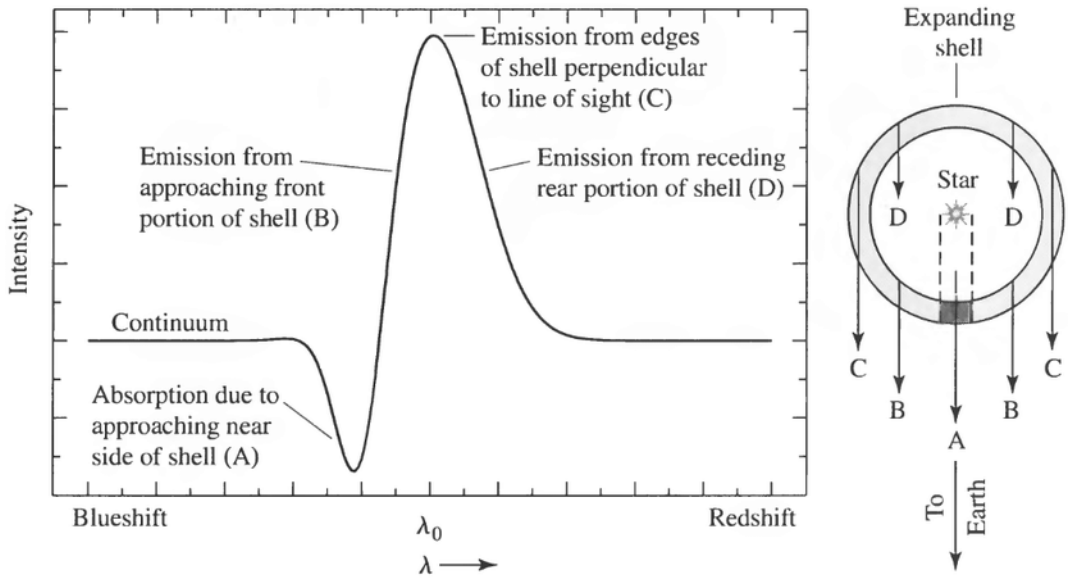

Figure 1.2: Example of a P-Cygni profile. Taken from Kasai (2013).

Spectral lines in Be stars

Classical Be stars exhibit different line profiles due to the different line-of-sight angles with respect to the axis of rotation of the star (see figure 1.3). Its classification is mainly divided into three types: pole-on stars, ordinary Be stars and Be-shell stars.

Pole-on stars have narrow, single-peak emission lines superimposed on photospheric absorption lines. Ordinary Be stars have double-peak emission line profiles, because the violet component of the profile forms in the approaching parts of the rotating envelope and the red component in the receding parts. On the other hand, Be-shell stars have sharp and deep absorption components in the centers of the double-peak emission lines. These absorption profiles form in the optically thick parts of the envelopes that face the stellar disk (Kogure & Leung 2007).

Absorption lines caused by the stellar wind are observed in the ultraviolet spectral region of Be stars, distinguished from photospheric absorption lines by their high excitation and high terminal velocities. These lines tend to show asymmetric profiles

that extend towards the violet side, due to the low gas density of the stellar winds. Additionally, due to their smaller terminal velocities in comparison with O stars, the X-ray emission is softer than that of O-type stars (Kogure & Leung 2007).

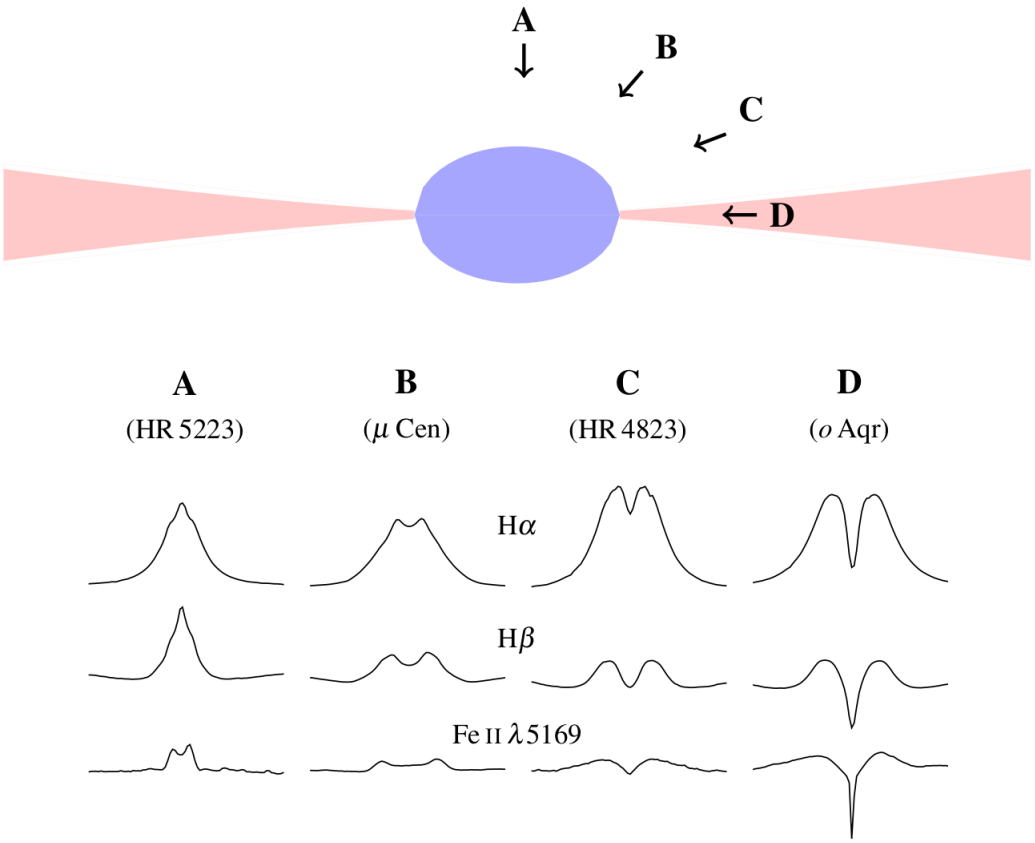

Figure 1.3: In the case of Be stars, due to the presence of the disk, their spectral lines depend of the angle of observation. Figure taken from Rivinius et al. (2013).

1.2 Aims

The general aim of this work is to obtain a wind velocity profile that adequately describes the winds of classical Be stars. Thus in Chapter 2, based on the modified standard theory of stellar winds (m-CAK theory), the physical effects experienced by fast rotating stars are discussed and the 1D stationary equation of motion (EoM) in the equatorial plane is presented. Chapter 3 presents the hydrodynamical codes HYDWIND and ZEUS-3D, which are the main computational tools in this work. Chapter 4 focuses on the study of the solutions of the 1D stationary EoM in the equatorial

plane, considering models with quasi-Keplerian rotation in the hydrodynamic code HYDWIND (Curé 2004). However, although currently are known three types of solutions for this EoM (fast, Ω-slow and δ-slow solutions), for purposes of this work we do not include the δ-slow solutions. Additionally, this section analyzes the conditions in which fast and Ω-slow solutions can co-exist and in which conditions they cease to co-exist. Finally, time-dependent models with quasi-Keplerian rotation are also exposed, solved with the ZEUS-3D code. Chapters 5 and 6 present the discussion of the results and the conclusions, respectively.

CHAPTER 2

Fast rotating massive stars

As mentioned, our object of study are classical Be stars, also called only Be stars. Furthermore, we previously mentioned some features of these fast rotating massive stars, but in this chapter we are going to delve into other features. First of all, we are going to present the physical effects that Be stars could experience due to their high rotations. After, we are going to focus in their winds, considering that Be stars have an outflowing gaseous disk in the equatorial plane, called decretion-disk.

Because the decretion-disk probably is a consequence of their fast rotation and their high luminosities, the decretion-disk can be modeled as a rotating radiation driven wind based on the m-CAK theory through a 1D stationary, hydrodynamic EoM in the equatorial plane of the star, considering that on average, the instabilities in the photosphere of the star over time do not affect the final result. Finally, based on that argument, we are going to show the EoM for a rotating decretion-disk in the equatorial plane. Additionally, to study the quasi-Keplerian rotation of decretion-disks in the next chapters, we are going to consider a simulated viscosity parameter, called γ_{vis}, into the azimuthal velocity component of the EoM. Note that here we are going to study the disks of Be stars as equatorial winds rotating in a quasi-Keplerian way.

2.1 Effects of fast rotation in Be stars

2.1.1 Oblateness and Gravity Darkening

A non-rotating star has spherical shape and the higher their rotation speeds, the change in the shape of the star begins to be evident. The faster a star rotates, the more flattened it becomes. This is the oblateness effect, represented in figure 2.1, where the geometry of the stars change from spherical geometry to oblate geometry.

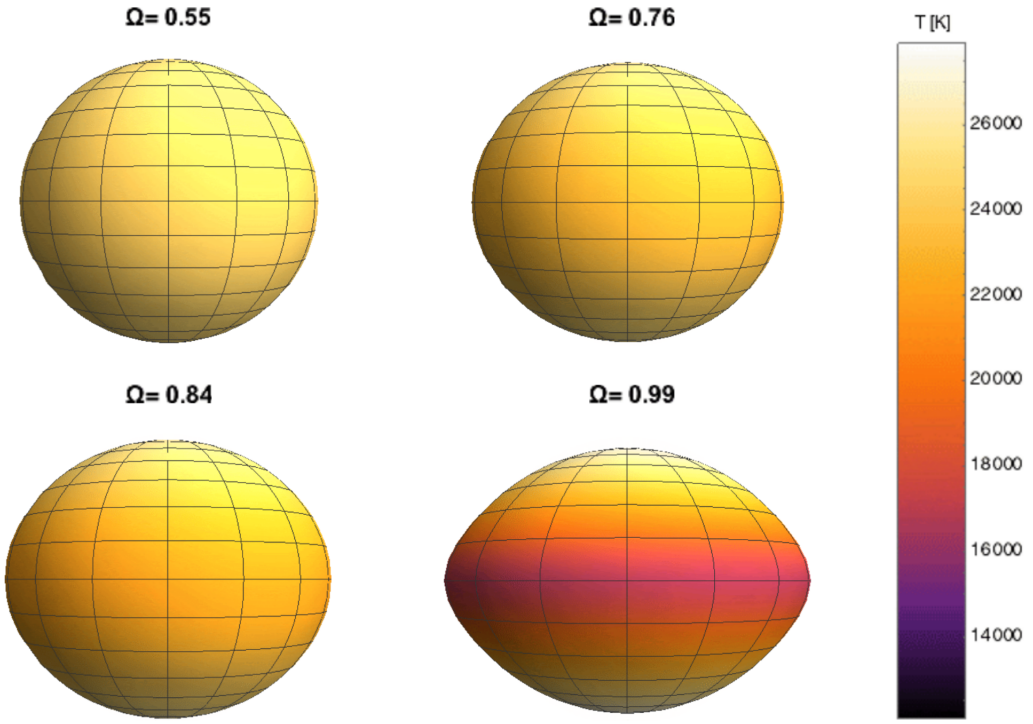

Figure 2.1: Illustrative example of a rotating star. The faster oblate shape and the difference of the effective temperature in poles and in the equator is evident. Here Ω is a parameter of rotation given in terms of the rotational speed on the equator of the star and its critical velocity: $\Omega = 0.99$ is a star very closely to its critical velocity and $\Omega = 0.0$ correspond to a non-rotating star. Each frame of the figure is part of a simulation created by I. Araya.

Although polar radius depends slightly on rotational velocity due to changes in internal structure of stars (Maeder 2009), this radius can be assumed to be independent of the rotational velocity because these changes are small. On the other hand, due to oblateness the effective gravity is modified, given place to a local effective gravity, which is dependent of the stellar latitude. These differences in effective

gravity are differences in radiative fluxes, because the flux is related to the radius of the star. Thus the maximum value of the effective temperature of stars occurs at their poles and the minimum value at their equators (von Zeipel 1924, Espinosa Lara & Rieutord 2011). This effect is known as the Gravity Darkening (GD), and it is shown in figure 2.1.

In this way, because Be stars are the fastest rotating non-degenerate stars, these stars are oblated and their equators are cooler than their poles. However, for the purpose of this work, in next calculations we only consider undeformed stars.

2.1.2 Decretion-disks

Long term observations have shown the appearance of emission lines, related to an equatorial outflowing circumstellar disk (also known as decretion-disk), in spectra of stars previously classified as B-type and the disappearance of emission lines in the spectra of stars previously classified as Be. Thus the presence of a decretion-disk in a Be star is the phenomenon that at some time gives a B-type star its classification as Be star. These results give rise to an unknown, but possibly related with some perturbation in the base of the wind of the star, mechanism of formation and/or dissipation of decretion-disks.

Considering the theory behind the radiation driven winds, as we said, the high luminosity in Be stars must be one of the main ingredients in the formation of decretion-disks. On the other hand, Araya et al. (2018) gave a possible explanation about the mechanism of formation and/or dissipation, arguing that a solution-switching between fast solutions and Ω-slow solutions may be a possible contributor of material injected into the circumstellar environment of Be stars, without requiring rotational speeds near critical values. Based on that, another probably mean ingredients in the formation (and/or dissipation) of a decretion-disk are the high rotational speeds of Be stars (also mentioned before) and a change of density in the equatorial plane.

Although other authors argue that the formation of the decretion-disks is not necessarily a consequence of the stellar winds of Be stars (Rivinius et al. 2013), we believe that the radiation driven winds theory can be good to model decretion-disks, due to

these type of disks are outflowing disks, as we previously mentioned. In this way, in the next section we describe the 1D equatorial hydrodynamic model for a rotating decretion-disk.

2.2 Hydrodynamical 1D model

2.2.1 Theory of radiation driven winds

It is known that stellar winds can be modeled as expanding stellar atmospheres. In the case of radiation driven winds, also called line driven winds, the absorption of photons in that expanding atmosphere plays a very important role. To explain how these type of winds work, this subsection take as reference Lamers & Cassinelli (1999).

First of all, to understand the physical process of photon absorption in radiation driven winds some assumptions are made: the atom always follow a radial direction, the speed with which the atom moves at the beginning (stellar surface) is much less than the speed of light ($v_r \ll c$) and the momentum of the atom is much greater than the momentum of the incoming photon in the frame of reference of an external observer ($h\nu_0 \ll mc$). That said, let's imagine an atom outside the photosphere moving radially out into space. On its way it absorbs a photon of frequency ν, which is going in its same direction. By conservation of linear momentum, the atom accelerates and its speed increases to: $v_r' = v_r + \frac{h\nu}{mc}$. The photon is then scattered with a frequency ν', i.e., the photon is re-emitted in a different direction than when it was absorbed, changing its frequency. In other words, the photon leaves the atom at an angle α with respect to the radial direction, such that the speed of the atom change to:

$$v_r'' = v_r' - \frac{h\nu'}{mc}\cos\alpha,$$

$$v_r'' = v_r + \frac{h\nu}{mc} - \frac{h\nu'}{mc}\cos\alpha. \tag{2.1}$$

If the photon absorbed and re-emitted have a frequency ν_0 in the rest frame of the atom, the frequency of the photon absorbed in the frame of reference of an external observer is $\nu = \nu_0(1 + v_r/c)$ and the frequency of the photon re-emitted is $\nu' = \nu_0(1 + v_r'/c)$. Substituting in the equation 2.1 and considering the assumptions previously mentioned, it is obtained that,

$$v_r'' = v_r + \frac{h\nu}{mc}(1 - \cos\alpha). \tag{2.2}$$

Now let's think that re-emission of many photons occurs randomly in the rest frame of the atom, then the mean transfer of momentum after the scattering of many photons will be:

$$\langle \Delta m v \rangle = \frac{h\nu_0}{c} \frac{1}{4\pi} \int_{-\frac{\pi}{2}}^{\frac{\pi}{2}} (1 - \cos\alpha) 2\pi \sin\alpha \, d\alpha = \frac{h\nu_0}{c}. \tag{2.3}$$

This equation tells us that the mean transfer of momentum, after many processes of absorption and re-emission, is equal to the momentum of the absorbed photons. This is impressive, as the entire process of photon absorptions and random re-emissions is reduced to just photon absorptions, that accelerate the wind!

Additionally, photons not only transfer momentum to the wind, they also transfer energy. Thus radiation provides the kinetic energy of the wind, the kinetic energy to carry the gas outside the gravitational potential barrier of the star and the thermal energy of the wind.

On the other hand, when modeling a radiation driven wind it is considered that there is a region in the wind called the coexistence region, which is different from the so-called co-existence region mentioned in the next chapters, where photons with a given frequency and coming from a given direction can interact with an ion, forming absorption lines. Here the only point along the photon path where the photon can interact with an ion in the wind is known as the Sobolev point and one way that turns out to be very convenient is to model the spectral lines using the Sobolev approximation, which considers the profile function equal to a δ function at the Sobolev point.

After estimating a radiative acceleration in the wind, given by a concept called force multiplier, it is important to consider additional points. First, it is necessary take into account that the star emits as a disk and not as a point object. Furthermore, since a photon is likely to be scattered not just once, but more times, it is more realistic to consider multiple scattering. And additionally, in the case of possible instabilities in the photosphere over time, these on average do not affect and the winds can be treated as stationary.

In the case of Be stars, stellar rotation is another important physical phenomenon to consider because when a star rotates rapidly it loses its spherical shape and GD effects become important (Gray 2005). Thus the effective temperature, which is an

observational parameter, becomes a function of the orientation angle. Sometimes, rotational speed at the equator of Be stars is so high that it is very close to its theoretical critical rotational speed. In these cases, the equatorial radius is much larger than the polar radius (see figure 2.1).

2.2.2 Hydrodynamic description of the wind

According to Lamers & Cassinelli (1999), the equation that describes the radial motion of gas in a stationary stellar wind follow the velocity gradient in Newton's law, in terms of the specific force (force per unit of mass). When only gas pressure and gravity are acting in the wind, the momentum equation reads:

$$v(r)\frac{dv}{dr} = -\frac{GM}{r^2} + \frac{1}{\rho}\frac{dP}{dr}, \tag{2.4}$$

where $v(r)$ is the radial component of the wind's velocity and $\frac{dv}{dr}$ is the velocity gradient along the radial coordinate. $v(r)\frac{dv}{dr}$ is given by the momentum of radiation absorbed per unit of volume and corresponds to the acceleration given by the sum of the gravitational acceleration of the star (GM/r^2) and the acceleration given by the gas pressure ($\rho^{-1}\frac{dP}{dr}$). Here we are going to omit values of physical constants and stellar parameters are going to be in their simple form: M (mass), R (radius), T (temperature), L (luminosity), etc.

However, winds of massive stars are driven by radiation. Additionally, the rotation of Be stars is not negligible. Thus other forces act in the wind and the EoM, based on de Araujo (1995), is the following:

$$v(r)\frac{dv}{dr} = -\frac{GM}{r^2} - \frac{1}{\rho}\frac{dP}{dr} + g_e(r) + g_L(r) + \frac{v_\phi^2(r)}{r}. \tag{2.5}$$

While

$$g_e(r) = \frac{GM}{r^2}\,\Gamma_e(r), \tag{2.6}$$

is the radiative acceleration due to electron scattering,

$$g_L(r) = \frac{\sigma_e}{4\pi c}\frac{L}{r^2}\,M(t)\,CF(r, v, \frac{dv}{dr}), \tag{2.7}$$

is the radiative acceleration due to lines; where

$$\Gamma_e(r) = \frac{\sigma_e(r)L}{4\pi cGM}, \tag{2.8}$$

is the ratio between the electron scattering force and the gravitational force, and

$$M(t) = k\, t^{-\alpha} \left[\frac{10^{-11} n_e}{W(r)}\right]^{\delta}, \tag{2.9}$$

is the force multiplier. The parameters k, α and δ are known as the force multiplier parameters (or line-force parameters). n_e is the electron density.

$$t \equiv \sigma_e(r)\, v_{th}\, \rho\, \frac{dr}{dv}, \tag{2.10}$$

is the dimensionless optical depth parameter introduced by Castor (1974); v_{th} is the thermal velocity of the protons and $\sigma_e(r)$ is some reference value for the electron-scattering opacity. In this work we used $\sigma_e(r) = \sigma_E = \sigma_T\,(n_e/\rho)$, which is the Thomson scattering absorption coefficient per density. σ_T is the Thomson cross-section of electrons.

$$W(r) = \frac{1}{2}\left[1 - \sqrt{1 - \left(\frac{R}{r}\right)^2}\right], \tag{2.11}$$

is the geometrical dilution factor and

$$CF(r, v, \frac{dv}{dr}) = \frac{2}{1-\mu_*^2}\int_{\mu_*}^{1}\left(\frac{(1-\mu^2)\,\frac{v}{r} + \mu^2\frac{dv}{dr}}{\frac{dv}{dr}}\right)^{\alpha}\mu d\mu, \tag{2.12}$$

is the finite disk correction factor, where

$$\mu_*^2 = 1 - \left(\frac{R}{r}\right)^2. \tag{2.13}$$

Additionally, the rotation centrifugal term $v_\phi^2(r)/r$ gives the centrifugal acceleration, where

$$v_\phi(r) = \Omega\sqrt{\frac{GM(1-\Gamma_e(r))}{R}}\left(\frac{R}{r}\right)^{\gamma_{\rm vis}}. \tag{2.14}$$

The equation 2.14 is the rotational velocity component of the wind in the equatorial plane, which is given by the conservation of angular momentum: $v_\phi(r)\, r = v_{rot}\, R$, when $\gamma_{vis} = 1$. Because $\gamma_{\rm vis}$ is a parameter that changes the specific angular momentum of the wind, such a torque provided by viscous shear, $\gamma_{\rm vis}$ is a parameter that simulates viscosity (Rivinius et al. 2013). Thus the kinematics of the disk changes with $\gamma_{\rm vis}$, such that the angular momentum is conserved when $\gamma_{\rm vis} = 1.0$, a Keplerian disk is described by $\gamma_{\rm vis} = 0.5$ and $\gamma_{\rm vis} = -1.0$ is for solid body rotation. $\gamma_{\rm vis}$ was previously introduced by de Araujo (1995) and he called it δ; for more details see de Araujo et al. 1994 and Stee & de Araujo 1994).

$$\Omega = \frac{v_{rot}}{v_{crit}} \tag{2.15}$$

is the stellar rotation rate in terms of the critical rotation speed, defined as the photospheric rotation velocity at which the centrifugal acceleration ($\omega^2 R = v_{rot}^2/R$) is equal to the effective acceleration of gravity:

$$v_{crit} = \sqrt{\frac{GM(1-\Gamma_e(r))}{R}}.^{1} \tag{2.16}$$

From now on, we are going to omit the dependency on r of the previous equations. Then if we substitute variables and rearrange terms, we obtain the final 1D equatorial hydrodynamic model for decretion-disks:

$$\begin{aligned}\left[1-\frac{a^2}{v^2}\right] r^2\, v\frac{dv}{dr} + GM(1-\Gamma)\left[1-\Omega^2\left(\frac{R}{r}\right)^{\mathbf{2\gamma_{vis}-1}}\right] \\ -2a^2 r - C\left(r^2 v\frac{dv}{dr}\right)^{\alpha} CF(r,v,\frac{dv}{dr})\left[\frac{10^{-11}n_e}{W(r)}\right]^{\delta} \;=\; 0,\end{aligned} \tag{2.17}$$

with

$$\Gamma = \frac{\sigma_E L}{4\pi c G M}, \tag{2.18}$$

and

$$C = \Gamma G M\, k\left(\frac{4\pi}{\sigma_E\, v_{th}\dot{M}}\right)^{\alpha}, \tag{2.19}$$

as constants. Here Γ is the classical Eddington factor and C is the eigenvalue of the solution. $\dot{M}/4\pi = r^2\rho\, v$ is the mass flux per unit of solid angle at the equator. P is the pressure, and is related to the density ρ and the isothermal sound speed a by $P = a^2\rho$, which is for an isothermal ideal gas.

Based on Curé (2004), we applied the following change of variables: $u = -R/r$, $w = v_r/a$ and $w' = \frac{dw}{du}$. Thus the equation 2.17 transforms into

$$\begin{aligned}F_A(u,w,w') \;\equiv\; &\left(1-\frac{1}{w^2}\right) ww' + A + \frac{2}{u} - a_{rot}^2(-u)^{\mathbf{2\gamma_{vis}-1}} \\ &-C'\, CF\, g(u)(w)^{-\delta}\left(ww'\right)^{\alpha} = 0,\end{aligned} \tag{2.20}$$

which is our EoM. Here

$$A = \frac{v_{esc}^2}{2a^2} = \frac{GM(1-\Gamma)}{a^2 R} = \frac{a_{rot}^2}{\Omega^2}, \tag{2.21}$$

[1] When a star deforms due to its high rotation, R is replaced by $R_{eq,\,max} = 3R_{pole}/2$, which is the maximum value that the radius at the equator can have when the star is rotating at the critical velocity ($\Omega = 1$). R_{pole} is the polar radius.

$$a_{rot} = \frac{v_{rot}}{a} = \frac{\Omega\, v_{crit}}{a} = \frac{\Omega}{a}\sqrt{\frac{GM(1-\Gamma)}{R}}, \tag{2.22}$$

$$C' = C\left(\frac{\dot{M}D}{2\pi}\frac{10^{-11}}{aR^2}\right)^{\delta}(a^2R)^{\alpha-1}, \tag{2.23}$$

$$D = \frac{n_e}{\rho} = \frac{(1+Z_{He}Y_{He})}{(1+A_{He}Y_{He})}\frac{1}{m_H}, \tag{2.24}$$

where Y_{He} is the relative helium abundance to hydrogen, Z_{He} is the quantity of free electrons provided by helium, A_{He} is the atomic mass number of helium and m_H is the proton mass. Additionally,

$$g(u) = \left(\frac{u^2}{1-\sqrt{1-u^2}}\right)^{\delta}. \tag{2.25}$$

The previous equations reflect the basis of the radiation driven winds theory in 1D. In Chapter 4 we study the behaviour of the solutions of equation 2.20, which will be solved using the hydrodynamical codes HYDWIND and ZEUS-3D, presented in the next chapter.

CHAPTER 3

Model hydrodynamic implementation

3.1 Stationary 1-D solutions using HYDWIND

In terms of time-averaged, mass loss rates and wind velocities are stables, thus stationary winds are adequate for describing radiation driven winds (Lamers & Cassinelli 1999). Curé (2004) propose the following EoM for stationary line driven winds,

$$F_C(u, w, w') \equiv \left(1 - \frac{1}{w^2}\right) ww' + A + \frac{2}{u} + a_{rot}^2 u - C'\, CF\, g(u)(w)^{-\delta} \left(ww'\right)^{\alpha} = 0. \quad (3.1)$$

This equation is equal to equation 2.20, but considering angular momentum conservation ($\gamma_{\text{vis}} = 1.0$). Therefore, all the terms in this equation have already been defined in the previous chapter. See section 2.2.2 for more details.

Based on the work of Curé (2004), HYDWIND is a one-dimensional stationary hydrodynamic code written in FORTRAN, that use a finite-difference method to solve the nonlinear differential equation 3.1. This finite-difference method uses a trial solution as initial guess, being relaxed toward the numerical solution by means of the Newton method (Araya & Curé 2020, and references therein).

Because equation 3.1 are developed based on the theory of CAK (Castor et al. 1975), FA (Friend & Abbott 1986) and PPK (Pauldrach et al. 1986), HYDWIND gives us the option to choose the line-force parametrization we want to use. While CAK theory assume the star as a non-rotating point source of radiation ($v_\phi = 0\,km/s$ and $CF(r, v, \frac{dv}{dt}) = 1$), PPK and FA theories are improvements of CAK theory, where is implemented a correction factor for the finite size of the star and the centrifugal force due to the rotation of the star. The difference between the last two theories is that PPK take into account the force multipliers calculated by Abbott (1982). In this way, $\delta = 0$ in CAK and FA theories. We used PPK theory in this work.

The installation of HYDWIND in the computers is not very complicated and is well explained in the *User Guide for Hydwin manual* of Araya & Curé (2020). After the creation of the executable the user only require to define the star model and after that, run the code. HYDWIND's input file is called for011.dat and it is composed for 11 rows and each row could have from 2 to 5 input parameters. These are show and defined in Araya & Curé (2020). If model converged, HYDWIND will generate two output files: for002.dat and for007.dat. The first of these output files contains a summary of all inputs and outputs parameters from the calculated model, and the last one contains the results from the calculations in different columns.

On the other hand, in order to investigate the behavior of the solutions in the equatorial plane of the hydrodynamic equations from the standard model of stellar winds driven by radiation of massive stars with high rotation, the work of de Araujo (1995) and Curé (2004) were connected. This connection resulted in the implementation of the empirical viscosity parameter $\gamma_{\rm vis}$ term in the EoM (subsection 2.2.2) and in the singularity and regularity conditions (appendix A). Aditionally, these equations were implemented in the HYDWIND code to be used as the main tool to obtain the corresponding numerical solutions of the EoM. For this new version of HYDWIND, $\gamma_{\rm vis}$ was added to the input file for011.dat (see table 3.1).

With the new version of HYDWIND, we initially calculated the standard model from de Araujo (1995) to verify that our results coincided with those obtained by him. For this purpose we consider the same line-force parameters α and k. The standard model represent a dimensionless point source star with a boundary condition $\rho_0 = 1.0x10^{-11}\,g\,cm^{-3}$ and Keplerian rotation ($\gamma_{\rm vis} = 0.5$) at $\Omega = 0.66$. For stellar

ROWS	PARAMETERS				
1	Model Name	F	F	F	
2	$T_{\rm eff}$	$log\ g$	R_*	Ω	
3	k	α	δ	$\gamma_{\rm vis}$	
4	1.0	Z_{He}			
5	ppk	sp	F	F	
6	den	Value 1			
7	r_i	r_n	n		
8	90	90	0		
9	1e-6	1e-3			
10	T	T	F	F	
11	Trial v(r)	β	v_∞	C'	Flag 9

Table 3.1: HYDWIND template from the input file for011.dat. The parameters that usually varies from one star model to another are effective temperature ($T_{\rm eff}$ [K]), superficial gravity ($log\ g$), radius (R_* [$R_\odot$]), normalised rotation speed (Ω), line-force parameters (k, α y δ), $\gamma_{\rm vis}$, number of free electrons provided by helium (Z_{He}), lower boundary condition (den: surface mass density and its Value 1), initial zone in the mesh (r_i [R_*]), last zone in the mesh (r_n [R_*]), number of zones in the mesh (n), trial velocity law ($v(r)$) and its values (β, v_∞ [km/s] and C') and the possibility for add more trials v(r) with the Flag 9.

parameters, we focused in the B0-B1 V-IV type star with $T_{\rm eff} = 25000$ K, $R_* = 10\ R_\odot$ and $log\ g = 3.6$. The results of this test model are shown in table 4.1.

We could not reproduce the solutions of de Araujo (1995) with $\alpha < 0.2$ because our models did not converge. On the other hand, mass fluxes and terminal velocities ratios show interesting results depending on the value of α. While mass fluxes ratios shows a steeper rise, terminal velocities ratios seem not to change. After confirm that the new version of HYDWIND reproduced partially de Araujo's results, we were able to calculate other stellar models.

3.2 Time dependent 1-D solutions using ZEUS-3D

Because sometimes HYDWIND do not converge, we decided to address this problem implementing $\gamma_{\rm vis}$ to a previous adapted version used in Araya et al. (2018) of the powerful time-dependent hydrodynamic code ZEUS-3D; which is a multi-physics

α	k	$\dot{M}_H/4\pi$ $[M_\odot/yr\,sr^{-1}]$	$v_{\infty,H}$ $[km/s]$	$\dot{M}_H/\dot{M}_A$	$v_{\infty,H}/v_{\infty,A}$
0.5	0.3	$4.278x10^{-9}$	1157	1.185	0.977
0.4	0.3	$5.975x10^{-10}$	832.7	1.269	0.976
0.4	0.5	$2.128x10^{-9}$	837.2	1.244	0.976
0.4	0.7	$4.912x10^{-9}$	840.4	1.289	0.976
0.3	0.3	$2.581x10^{-11}$	601.7	1.426	0.974
0.3	0.7	$4.288x10^{-10}$	607.9	1.474	0.974
0.3	1.5	$5.360x10^{-9}$	614.4	1.445	0.975
0.2	0.3	$6.060x10^{-14}$	415.6	1.888	0.973
0.2	1.5	$1.826x10^{-10}$	426.5	1.920	0.974
0.2	3.2	$7.875x10^{-9}$	433.6	1.916	0.974

Table 3.2: $\dot{M}_H/4\pi$ is the mass flux per unit of solid angle in the equatorial plane $[M_\odot/yr\,sr^{-1}]$ and $v_{\infty,H}$ is the terminal velocity $[km/s]$, both from HYDWIND. Thus, $\dot{M}_H/\dot{M}_A$ is the ratio of mass flux in the equatorial plane between HYDWIND and de Araujo (1995) results, respectively. In the same way, $v_{\infty,H}/v_{\infty,A}$ is the ratio of terminal velocities.

computational fluid dynamics code written in FORTRAN, able to solve the EoM 3.1 in a non-stationary regime (Clarke 1996). In other words, this time-dependent code converges in time to a stationary solution. Henceforth, ZEUS-3D will be mention only as ZEUS.

In this adapted version of ZEUS we can use HYDWIND outputs for007.dat as its initial condition to calculate the solutions to the EoM. Taking into account the previous information, we compared some models with different values of $\gamma_{\rm vis}$ and Ω, calculated with both HYDWIND and with ZEUS to confirm that the migration from HYDWIND to ZEUS had been carried out properly. After successful tests, we proceeded to calculate other stellar models.

ZEUS input file is called *inzeus* and table 3.2 shows an example of inzeus for a star model with $\gamma_{\rm vis} = 1.0$. In this work, the parameters that were totally or partially modified depending on the model being studied are: R_* (x1min and rstsu), the maximum distance to calculate (x1max $[R_\odot]$), the physical time in which the execution stops (tlim), the mass of the star (ptmass), the isothermal speed of sound (ciso), the time interval that passes between each ZEUS output (dtusr = tlim/number of outputs), the density in the base of the wind (dwind), the HYDWIND input file (nfile), the number

of data from HYDWIND file (nd and nbl), $T_{\rm eff}$ (twind), Ω (comega), α (alphai), $\bar{Q}$ from Gayley (1995) (qbar), δ (delta), the star's luminosity (lstsu [$L_\odot$]) and $\gamma_{\rm vis}$ (gamvis). Almost all of these input parameters can be found in the output file for002.dat of HYDWIND.

ROWS	PARAMETERS	
1	$iocon	$
2	$rescon	dtdmp= -3.6e5, id= 'cm', resfile= 'zr00cm' $
3	$ggen1	nbl= 500, x1min= 6.93, x1max= 693.0, igrid= 1, x1rat= 1.02
4		, x1scale= 6.9598e10, lgrid= .t. $
5	$ggen2	nbl= 1 , x2min= 0.0 , x2max= 1.0 , igrid= 1, x2rat= 1.
6		, units= 'pi' , lgrid= .t. $
7	$ggen3	nbl= 1 , x3min= 0.0 , x3max= 2.00 , igrid= 1, x3rat= 1.
8		, units= 'pi' , lgrid= .t. $
9	$pcon	nlim= 100000000, tlim= 5.0e7, ttotal= 72000., tsave= 1.0 $
10		
11	$edcon	$
12	$hycon	qcon= 0.2, qlin= 0.0, courno= 0.5, iord= 2, istp= 0,
13		icool= 0, itote= 0, dtrat= 1.e-3 $
14	$iib	niib(1:1,1:1)= 3 $
15	$oib	noib(1:1,1:1)= 2 $
16	$ijb	nijb(1:1,1:1105)= 4 $
17	$ojb	nojb(1:1,1:1105)= 4 $
18	$ikb	nikb(1:1105,1:1)= 4 $
19	$okb	nokb(1:1105,1:1)= 4 $
20	$grvcon	g= 6.67d-8, ptmass= 3.069e34, x1ptm= 0.0, x2ptm= 0.0,
21		x3ptm=0.0 $
22	$eqos	rgas= 1.0, gamma= 1.01, niso= 1, ciso= 19.00e5 $
23	$gcon	$
24	$sscon	$
25	$plt1con	$
26	$plt2con	$
27		ipixdir= 2, dtpix= 0.000
28		, pixvar= 'd'

Continues on the next page.

ROWS	PARAMETERS	
29	, nlpix= 300	
30	, pixmin= 1.0e-29	
31	, pixmax= 1.20e-23	
32	, ipixmm= 0	$
33	$voxcon	$
34		
35		
36	$usrcon dtusr= 5.0e5	$
37	$hdfcon dthdf= 1.0e0, hdfvar= 'to'	$
38	$tslcon dttsl= 1.0e4, dttslp= 1.0e4	$
39	$discon	$
40	$radcon	$
41	$pgen dwind= 8.709e-11, case1= 0, xml= 0, file= 1,	
42	nfile='44-F-b2_vi700_vp70-for007.dat', nd= 500, vwind= 0.0,	
43	angle= 90.0, twind= 27800.d0, comega= 0.70, Vinf= 0.0,	
44	beta= 0.0, alphai= 0.545, qbar= 4778.0d0, delta= 0.05,	
45	rstsu= 6.93, lstsu= 2.588d4, sigele= 0.3129, dvr = 2,	
46	seed= 1, timer1= 0.0, timer2= 0.0,	
47	min= 0.0, max= 0.0, optn= 0, gamvis=1.00	$

Table 3.3: Example of an ZEUS input file with $\gamma_{\rm vis}$ implementing. All units are in the cgs system and bold font parameters corresponds to the parameters that were totally or partially modified depending on the model being studied. For more details regarding the rest of the parameters, see Clarke (1996).

ZEUS 1-D output files are called zutnnn, where nnn corresponds to the number of output file, from 000 to nnn. Each output file have 10 columns, among which is the radial coordinate column in cm, wind velocity column in km/s and the wind density column in $g\,cm^{-3}$. This fact makes it possible for convert the last ZEUS output into a type for007.dat file for use it as an initial guess to calculate solutions in an iteractive way, changing just one parameter to study the behaviour of fast solutions and Ω-slow solutions with ZEUS. Thus we only concentrate on changing Ω to study the behavior of fast solutions and Ω-slow solutions within the co-existence region through the analysis of the velocity profile, of the velocity gradient, of the mass loss rate, among others.

To test that the migration from HYDWIND to ZEUS had been carried out properly, we compared some models of the B2.5 V type star calculated with both codes, using different values of $\gamma_{\rm vis}$ and Ω. Figure 4.10 shows an example of these models.

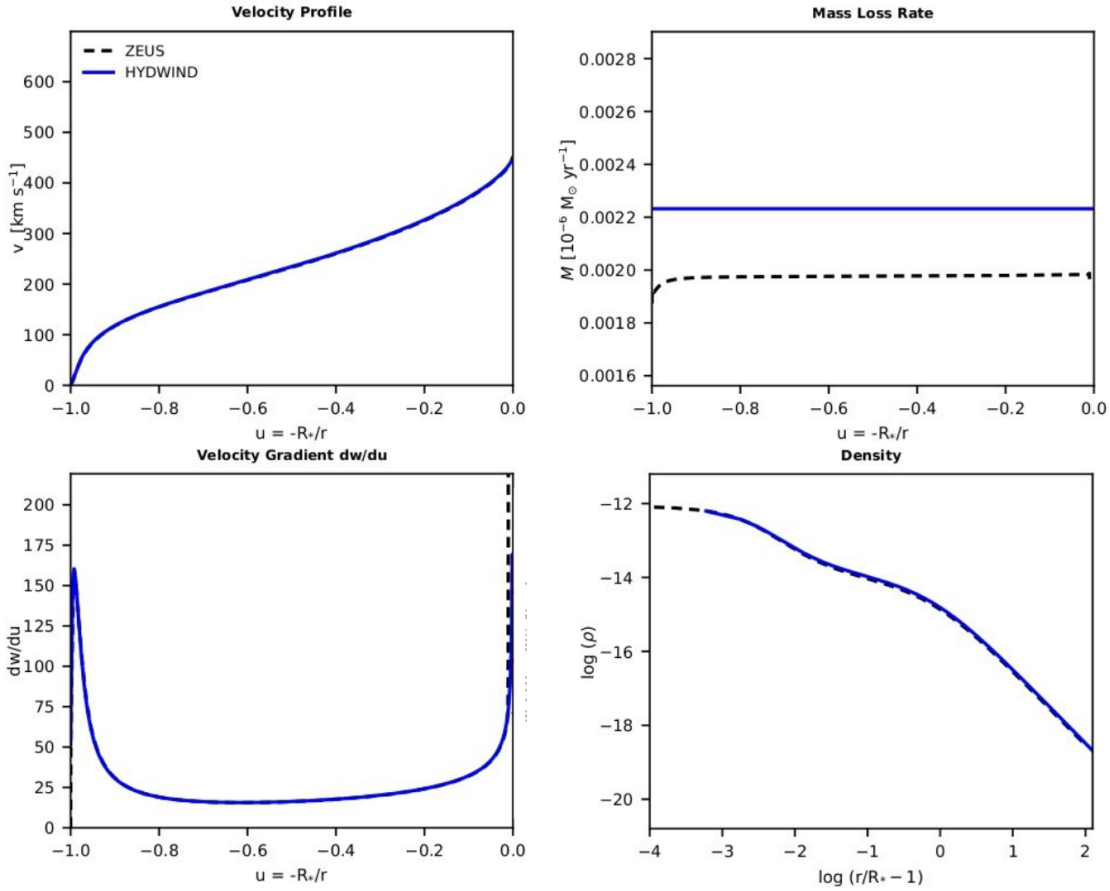

Figure 3.1: Comparison between results of velocity profile, velocity gradient, mass loss rate and density from HYDWIND (blue solid curves) and from ZEUS (black dashed curves). These results correspond to B2.5 V star model, with $\gamma_{\rm vis} = 0.85$ and $\Omega = 0.75$.

CHAPTER 4

Results

4.1 Searching low terminal velocities

Observational results show that the terminal velocities of the winds of classic Be stars are lower than the terminal velocities found theoretically so far. Because of this, after confirming that the new version of HYDWIND reproduced similar results to de Araujo's results, our main goal was to find the lowest terminal velocities for star models B2 V and B2.5V, considering different values of γ_{vis}.

Before going into the details of these models, we have to clarify that although we know that strictly speaking the line-force parameters must be calculated in a self-consistent way (Gormaz-Matamala et al. 2019), in this work we followed the procedure of de Araujo (1995), taking these parameters freely. Additionally, in this work we assumed only spherical symmetry, thus ruling out the Oblate and GD effects (subsection 2.1.1). Therefore, our results could change in the future, if the line-force parameters are calculated in a self-consistent way and/or if we take into account the oblate shape due to the high rotation and the GD effect.

First we computed a B2 V star model, with stellar parameters and line-force parameters shown in table 4.1. For this case we used $\Omega = 0.99$ and $\gamma_{\rm vis} = 0.52$. for this model we obtained a terminal velocity $v_\infty = 106.2\,km/s$ at $100\,R_*$ and a mass loss rate

$\dot{M} = 1.422x10^{-8}\, M_{\odot}/yr$. Figure 4.1 show the velocity profile of this B2 V star model, which correspond to an Ω-slow solution. From here is evident that we can obtain low terminal velocities when we study the quasi-Keplerian regime.

$\mathbf{T_{eff}}$ [K]	$\mathbf{R_*}$ $[R_\odot]$	**log g**	**k**	$\boldsymbol{\alpha}$	$\boldsymbol{\delta}$	$\boldsymbol{\rho_0}$ $[g\ cm^{-3}]$
21000	4.00	4.50	0.32	0.50	0.00	$5.0x10^{-10}$

Table 4.1: Stellar and line-force parameters of a B2 V type star.

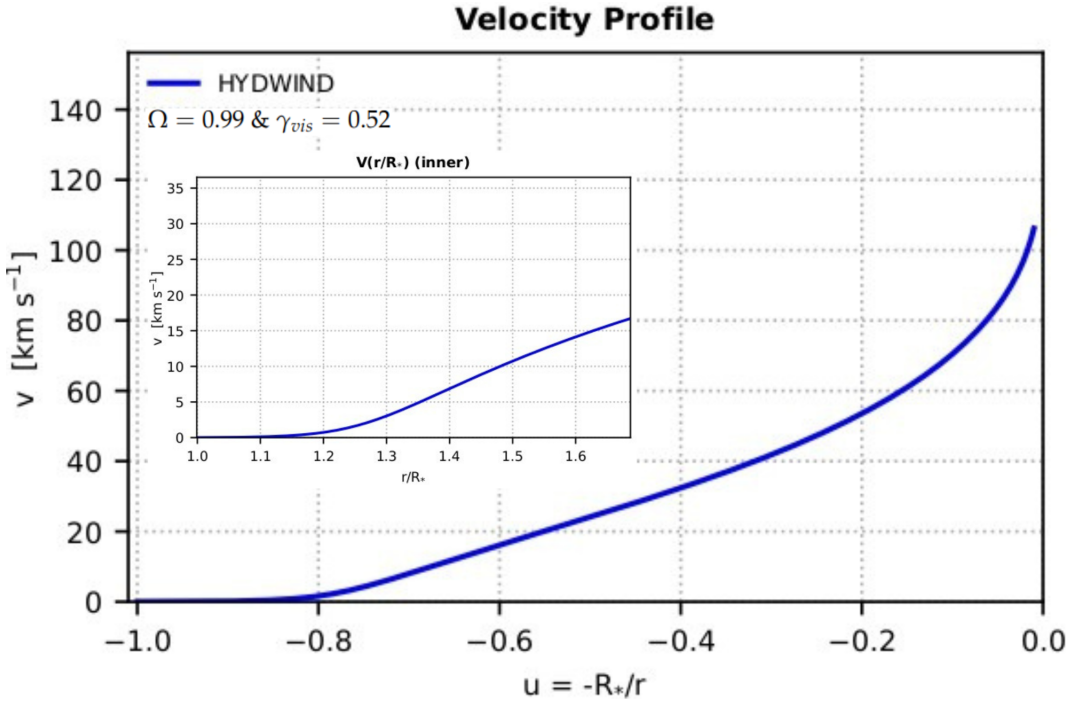

Figure 4.1: Velocity profile of a B2 V star model as function of $u = -R_*/r$. The inset is a zoom just above the surface, but with $r/R_* = -1/u$ in the X-axis.

For the B2.5 V star we calculated a series of models, considering different values of Ω (in the range from 0.50 to 0.99) and $\gamma_{\rm vis}$ (in the range from 0.50 to 1.00). Stellar and line-force parameters are shown in the following table:

$\mathbf{T_{eff}}$ [K]	$\mathbf{R_*}$ $[R_\odot]$	**log g**	**k**	$\boldsymbol{\alpha}$	$\boldsymbol{\delta}$	$\boldsymbol{\rho_0}$ $[g\ cm^{-3}]$
20000	4.00	4.11	0.61	0.50	0.00	$8.709x10^{-13}$

Table 4.2: Stellar and line-force parameters of a B2.5 V type star from Araya et al. (2018).

Also, to obtain lower terminal velocities, we follow the conclusion of de Araujo (1995), where lower terminal velocities could found taking lower values of α. Based

on that conclusion, we calculated more solutions for the previous star model with $\alpha = 0.45$ and $\alpha = 0.40$. However, many solutions did not converge when $\alpha = 0.40$. Thus, we discard values of $\alpha < 0.45$ and we only concentrated in the solutions of the models with $\alpha = 0.50$ and $\alpha = 0.45$. Results are shown in tables 4.3, 4.4, 4.5 and 4.8.

These tables show that low terminal velocities are obtained with low α values, low $\gamma_{\rm vis}$ values and high Ω values. However, as figures 4.3 and 4.4 show, with those values the initial speed of the wind is close to the isothermal sound speed. In other words, the speed of the wind in the surface of the star acquires very high values that do not agree with the theory of isothermal winds, and this is not physically acceptable.

To clarify that this result was not an error by Hydwind, we decided to used ZEUS. For this purpose we used the hydrodynamic results obtained previously with HYDWIND in section 4.1 ($\alpha = 0.45$, $\Omega = 0.99$ and $\gamma_{\rm vis} = 0.5103$) as initial condition. The results are shown graphically in figure 4.2, where the initial velocity of the wind still being close to the isothermal sound speed.

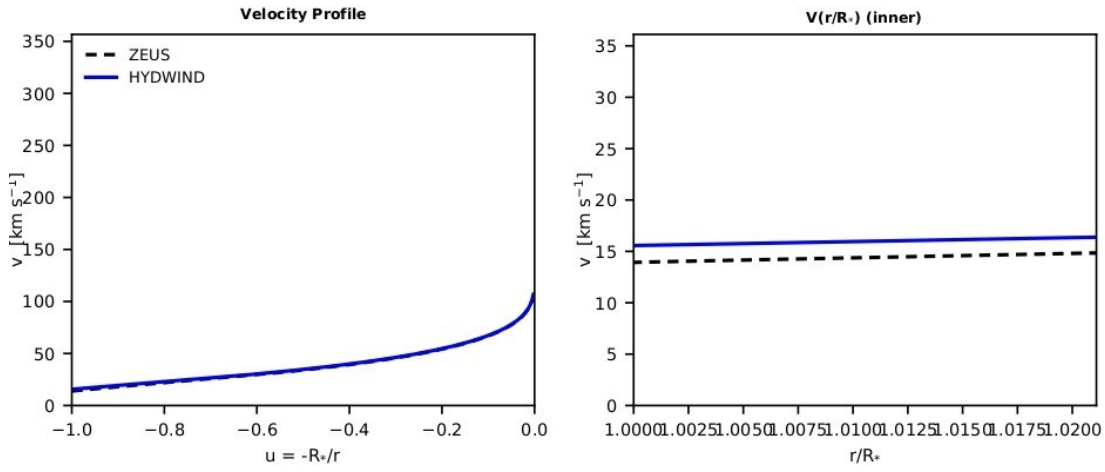

Figure 4.2: Comparison between velocity profiles obtained with HYDWIND (blue solid curves) and with ZEUS (black dashed curves). These results correspond to the B2.5 V star model, with $\gamma_{\rm vis} = 0.5103$ and $\Omega = 0.99$.

We suspect that this result is due to the spherical symmetry adopted in this work, where we have not considered the oblateness and GD effects despite the high rotation rate used. In the next chapter we will to discuss it.

	Ω							
$\gamma_{\mathbf{vis}}$	**0.60**		**0.70**		**0.75**		**0.80**	
	$\mathbf{v_\infty}$ [km/s]	$\dot{\mathbf{M}}$ [$\mathbf{M_\odot/yr}$]	$\mathbf{v_\infty}$ [km/s]	$\dot{\mathbf{M}}$ [$\mathbf{M_\odot/yr}$]	$\mathbf{v_\infty}$ [km/s]	$\dot{\mathbf{M}}$ [$\mathbf{M_\odot/yr}$]	$\mathbf{v_\infty}$ [km/s]	$\dot{\mathbf{M}}$ [$\mathbf{M_\odot/yr}$]
1.00	*1426*	*1.590E-09*	*1184*	*2.011E-09*	487.8	2.149E-09	465.9	2.153E-09
0.95	*1431*	*1.592E-09*	*1193*	*2.015E-09*	475.6	2.168E-09	452.8	2.176E-09
0.90	*1437*	*1.594E-09*	*1202*	*2.020E-09*	462.3	2.194E-09	437.4	2.203E-09
0.85	*1443*	*1.595E-09*	*1213*	*2.024E-09*	449.3	2.232E-09	422.7	2.246E-09
0.80	*1450*	*1.597E-09*	*1225*	*2.029E-09*	428.8	2.248E-09	406.3	2.304E-09
0.75	*1458*	*1.599E-09*	*1239*	*2.033E-09*	*1096*	*2.390E-09*	390.3	2.392E-09
0.70	*1467*	*1.601E-09*	*1254*	*2.038E-09*	*1118*	*2.398E-09*	374.4	2.528E-09
0.65	*1477*	*1.603E-09*	*1272*	*2.042E-09*	*1142*	*2.406E-09*	363.0	2.697E-09
0.60	*1489*	*1.604E-09*	*1291*	*2.047E-09*	*1167*	*2.414E-09*	*1020*	*2.978E-09*
0.55	*1503*	*1.606E-09*	*1313*	*2.051E-09*	*1196*	*2.422E-09*	*1059*	*2.993E-09*
0.50	*1520*	*1.608E-09*	*1339*	*2.056E-09*	*1228*	*2.429E-09*	*1100*	*3.008E-09*

Table 4.3: Results of the solutions of the model of the B2.5 V type star mentioned previously for different values of Ω and $\gamma_{\rm vis}$, considering $\alpha = 0.50$. $\dot{M}$ is the mass loss rate in solar masses per year and v_∞ is the terminal velocity in km/s. Solutions whit slanted font style correspond to fast solutions and solutions with normal font style corresponds to Ω-slow solutions. For simplicity the table we omitted all the results of $\Omega = 0.50$ calculated, which are from fast solutions and the values of $\dot{M}$ and v_∞ are similar than results when $\Omega = 0.60$.

	Ω							
$\gamma_{\mathbf{vis}}$	**0.85**		**0.90**		**0.95**		**0.99**	
	$\mathbf{v_\infty}$ [km/s]	$\dot{\mathbf{M}}$ [$\mathbf{M_\odot/yr}$]	$\mathbf{v_\infty}$ [km/s]	$\dot{\mathbf{M}}$ [$\mathbf{M_\odot/yr}$]	$\mathbf{v_\infty}$ [km/s]	$\dot{\mathbf{M}}$ [$\mathbf{M_\odot/yr}$]	$\mathbf{v_\infty}$ [km/s]	$\dot{\mathbf{M}}$ [$\mathbf{M_\odot/yr}$]
1.00	445.6	2.161E-09	425.9	2.167E-09	407.0	2.173E-09	393.1	2.180E-09
0.95	430.8	2.185E-09	409.8	2.193E-09	390.1	2.203E-09	375.2	2.212E-09
0.90	414.5	2.218E-09	392.2	2.231E-09	370.3	2.239E-09	355.2	2.255E-09
0.85	397.8	2.264E-09	373.7	2.282E-09	350.9	2.300E-09	334.0	2.316E-09
0.80	379.5	2.331E-09	342.9	2.243E-09	328.4	2.386E-09	310.8	2.408E-09
0.75	360.2	2.428E-09	332.5	2.471E-09	305.4	2.511E-09	285.7	2.549E-09
0.70	340.8	2.583E-09	310.2	2.653E-09	280.2	2.722E-09	258.3	2.784E-09
0.65	322.9	2.841E-09	292.0	2.892E-09	258.5	3.001E-09	234.2	3.105E-09
0.60	323.6	2.857E-09	287.2	2.969E-09	252.4	3.096E-09	221.8	3.019E-09
0.55	*892.2*	*3.975E-09*	258.1	5.285E-09	200.2	6.363E-09	155.4	7.677E-09
0.50	*947.8*	*4.009E-09*	*761.4*	*6.119E-09*	*517.3*	*1.302E-08*	asound < v(0)	

Table 4.4: This table is the continuation of table 4.3. The phrase asound < v(0) correspond to a message of error when photosphere velocity is bigger than the isothermal velocity of sound.

γ_{vis}	Ω							
	0.60		0.70		0.75		0.80	
	v_∞ [km/s]	$\dot{M}$ [$M_\odot$/yr]	v_∞ [km/s]	$\dot{M}$ [$M_\odot$/yr]	v_∞ [km/s]	$\dot{M}$ [$M_\odot$/yr]	v_∞ [km/s]	$\dot{M}$ [$M_\odot$/yr]
1.00	*1176*	*4.590E-10*	454.4	5.617E-10	433.7	5.633E-10	413.9	5.650E-10
0.95	*1182*	*4.597E-10*	443.5	5.667E-10	422.0	5.697E-10	401.4	5.727E-10
0.90	*1188*	*4.604E-10*	433.2	5.750E-10	409.9	5.784E-10	386.8	5.807E-10
0.85	*1195*	*4.612E-10*	421.5	5.847E-10	397.0	5.903E-10	373.5	5.961E-10
0.80	*1204*	*4.619E-10*	*994.7*	*6.172E-10*	384.2	6.072E-10	357.5	6.130E-10
0.75	*1213*	*4.626E-10*	*1013*	*6.191E-10*	371.2	6.324E-10	343.4	6.434E-10
0.70	*1223*	*4.633E-10*	*1032*	*6.211E-10*	359.3	6.707E-10	328.7	6.886E-10
0.65	*1235*	*4.641E-10*	*1053*	*6.231E-10*	*933.0*	*7.601E-10*	316.6	7.658E-10
0.60	*1249*	*4.648E-10*	*1076*	*6.250E-10*	*966.1*	*7.637E-10*	310.6	9.085E-10
0.55	*1265*	*4.655E-10*	*1101*	*6.270E-10*	*999.7*	*7.672E-10*	*879.9*	*9.925E-10*
0.53	*1275*	*4.656E-10*	*1115*	*6.275E-10*	*1016*	*7.684E-10*	*900.8*	*9.952E-10*
0.5103	*1282*	*4.659E-10*	*1126*	*6.283E-10*	*1031*	*7.698E-10*	*919.3*	*9.980E-10*
0.50	*1283*	*4.662E-10*	*1129*	*6.289E-10*	*1036*	*7.707E-10*	*926.6*	*9.996E-10*

Table 4.5: The same as table 4.2 but with $\alpha = 0.45$. In order to show the lowest value we obtained for the terminal velocity, we added two extra rows for $\gamma_{vis} = 0.53$ and $\gamma_{vis} = 0.5103$.

γ_{vis}	Ω							
	0.85		0.90		0.95		0.99	
	v_∞ [km/s]	$\dot{M}$ [$M_\odot$/yr]	v_∞ [km/s]	$\dot{M}$ [$M_\odot$/yr]	v_∞ [km/s]	$\dot{M}$ [$M_\odot$/yr]	v_∞ [km/s]	$\dot{M}$ [$M_\odot$/yr]
1.00	395.4	5.675E-10	377.7	5.699E-10	360.9	5.722E-10	348.8	5.745E-10
0.95	381.5	5.756E-10	362.1	5.778E-10	344.9	5.819E-10	332.1	5.850E-10
0.90	366.2	5.859E-10	346.5	5.909E-10	327.8	5.955E-10	313.8	5.982E-10
0.85	350.9	6.018E-10	329.6	6.078E-10	309.1	6.139E-10	294.5	6.188E-10
0.80	333.9	6.234E-10	311.1	6.329E-10	289.7	6.421E-10	273.9	6.501E-10
0.75	317.3	6.572E-10	291.5	6.703E-10	268.1	6.844E-10	250.5	6.959E-10
0.70	299.8	7.098E-10	271.3	7.315E-10	245.1	7.543E-10	226.0	7.755E-10
0.65	283.1	8.014E-10	250.6	8.382E-10	219.2	8.733E-10	199.6	9.280E-10
0.60	271.1	9.801E-10	233.3	1.070E-09	194.6	1.159E-09	170.2	1.288E-09
0.55	*732.8*	*1.401E-09*	226.2	1.701E-09	175.4	2.140E-09	137.1	2.705E-09
0.53	*762.0*	*1.408E-09*	*584.7*	*2.338E-09*	174.1	3.362E-09	122.6	5.166E-09
0.5103	*787.0*	*1.415E-09*	*623.4*	*2.362E-09*	*401.9*	*5.888E-09*	111.8	2.045E-08
0.50	*797.5*	*1.419E-09*	*639.0*	*2.375E-09*	*430.4*	*5.985E-09*	asound < v(0)	

Table 4.6: This table is the continuation of table 4.5. The phrase asound < v(0) correspond to a message of error when photosphere velocity is bigger than the isothermal velocity of sound.

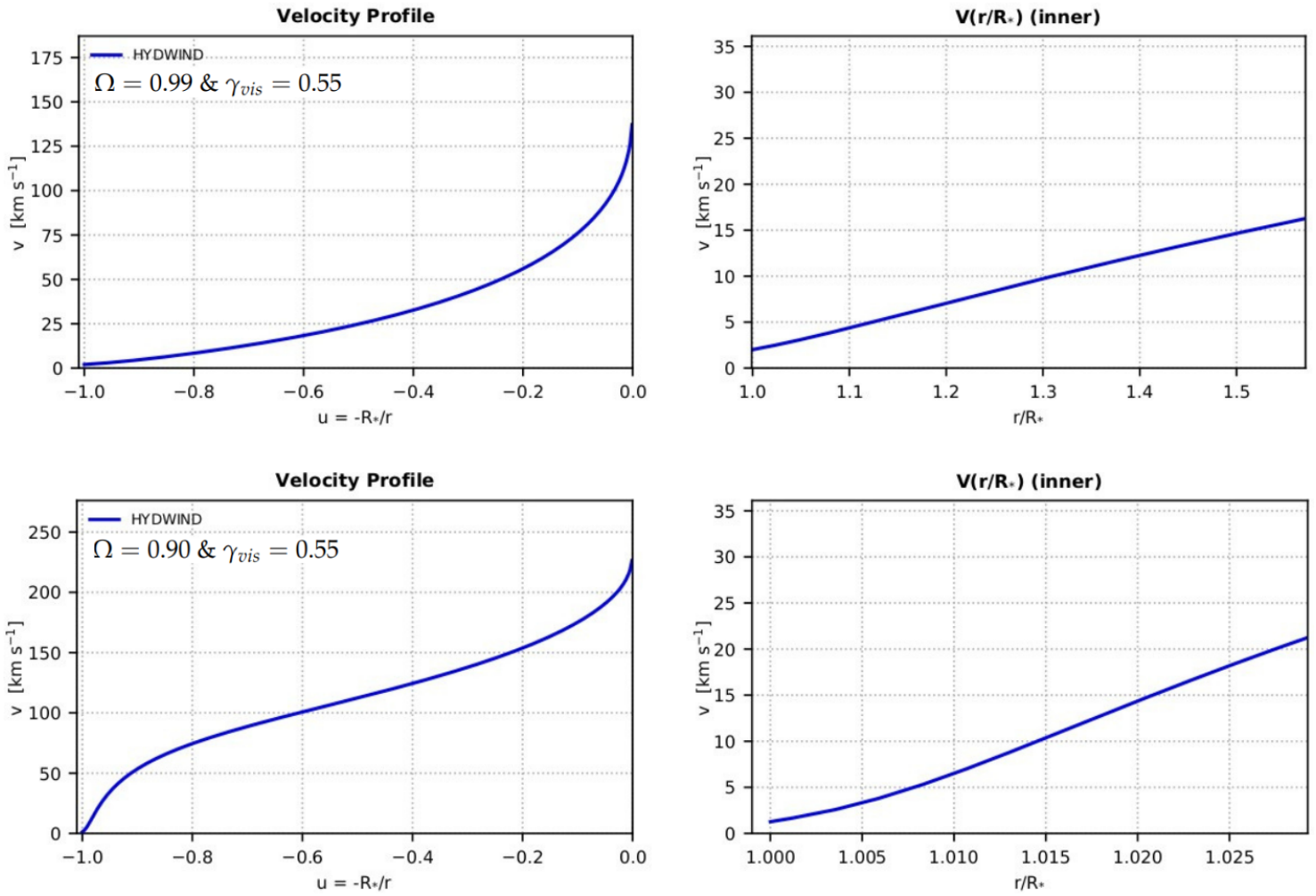

Figure 4.3: Velocity profiles of B2.5 V star model with $\alpha = 0.45$. The velocity of the wind in the surface of the star (v_0) increases when Ω increases.

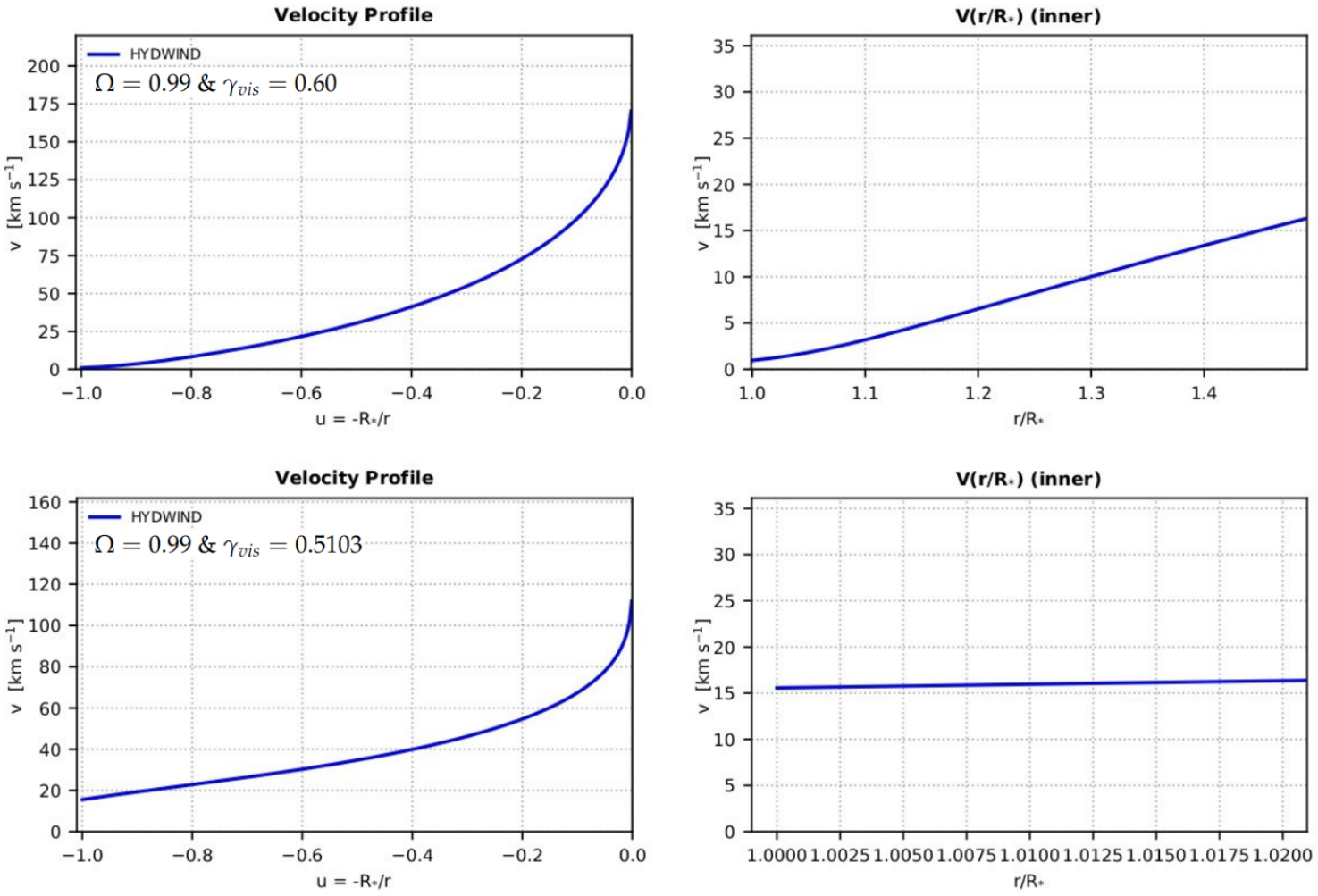

Figure 4.4: The same that previous plot, but keeping Ω constant and varying $\gamma_{\rm vis}$: at high rotational rate, v_0 increases when $\gamma_{\rm vis}$ decreases.

Although for this model the speed of the wind at the stellar surface is almost close to the sound speed when the star has high rotation rates in the quasi-Keplerian regime, we can analyse the rest of the results. Thus we plotted terminal velocities (v_∞) as a function of $\gamma_{\rm vis}$ and Ω, to analyze graphically the behavior of terminal velocity of the B2.5 V star model when $\alpha = 0.45$. Figures 4.5 and 4.6 show these plots, respectively.

From figure 4.5, the higher the Ω value, the lower the terminal velocity. As we expected, almost all of the solutions with slow terminal velocities were Ω-slow solutions. Also, a gap is evident between fast and Ω-slow solutions. From figure 4.6, terminal velocities lower than 200 km/s are found when $\gamma_{\rm vis} < 0.65$. Additionally, based on tables 4.3, 4.4, 4.5 and 4.8; the figure 4.7 shows a frequency plot of the fast solutions and the Ω-slow solutions with respect to $\gamma_{\rm vis}$ for $\alpha = 0.50$ and $\alpha = 0.45$. In this plot is visible that when $\gamma_{vis} \longrightarrow 0.5$, the number of fast solutions increases and the number of Ω-slow solutions decreases. This result was also confirmed in the topology analysis of the behaviour of fast and Ω-slow solutions, exposed in the appendix A.

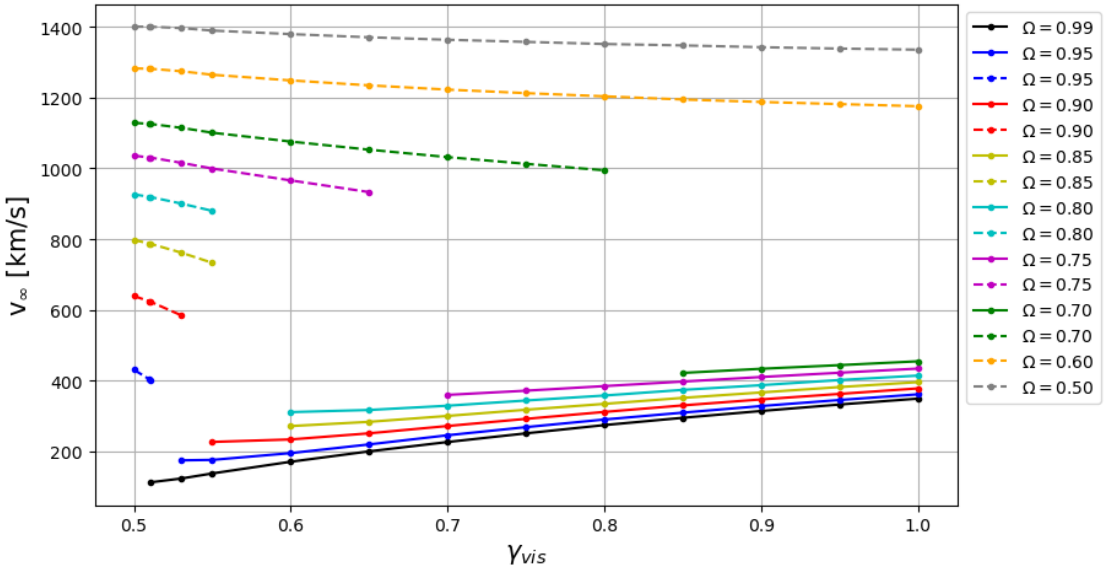

Figure 4.5: Each point belong to one cell from the tables 4.4 and 4.5, except the points belonging to $\Omega = 0.50$, which the corresponding results were omitted in these tables. Points of dashed lines correspond to fast solutions and points of solid lines correspond to Ω-slow solutions. For this range of Ω values, the lowest terminal velocities are found when $\Omega = 0.99$ (almost all of these solutions were Ω-slow solutions) and the higher terminal velocities are found when $\Omega = 0.50$ (all of these solutions were fast solutions).

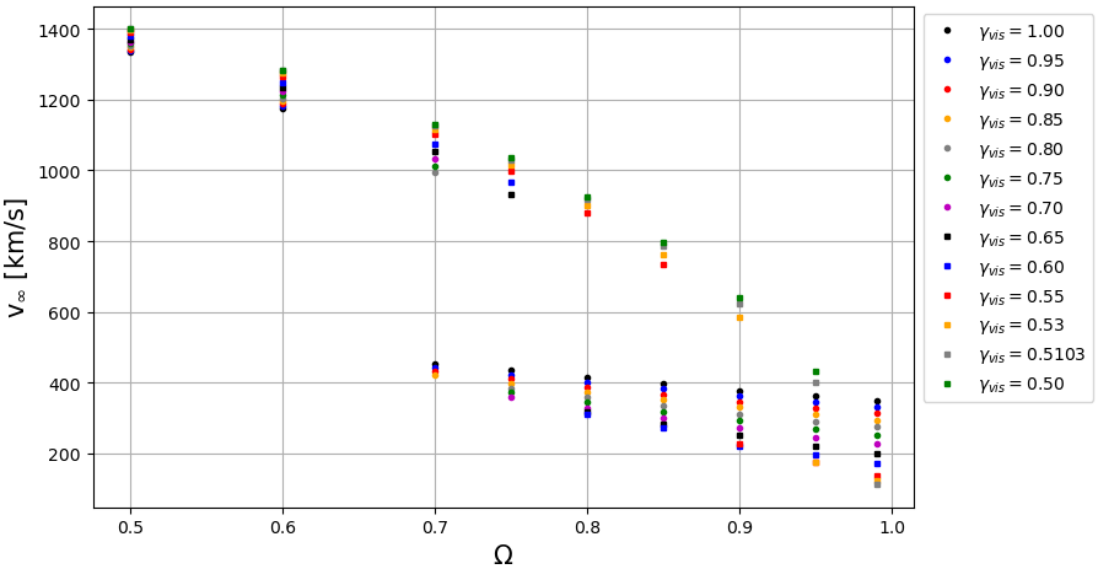

Figure 4.6: Terminal velocities lower than 200 km/s are found for high rotational velocities when $\gamma_{\text{vis}} < 0.65$. As figure 4.5, each point belong to one cell from the tables 4.4 and 4.5.

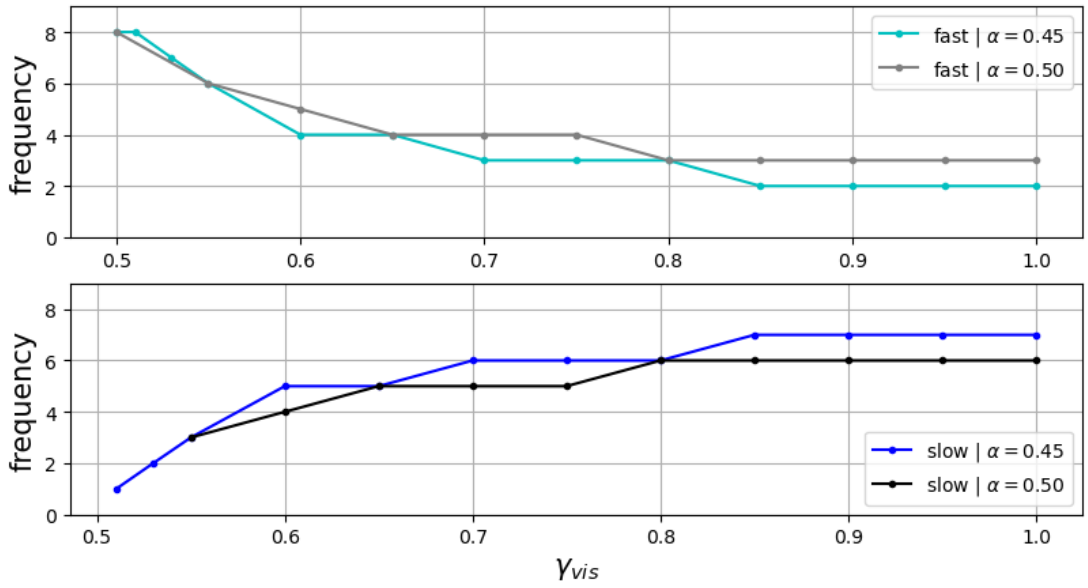

Figure 4.7: Frequency plot of number of solutions: fast solutions are shown in grey ($\alpha = 0.50$) and light blue ($\alpha = 0.45$). Ω-slow solutions are shown in black ($\alpha = 0.50$) and blue ($\alpha = 0.55$). Fast solutions begin to dominate when the star's rotation approaches to Keplerian rotation, whatever the nature of the lines driving the wind and regardless that the stellar rotation is very high. Furthermore, α value affects the number of fast solutions and the number of Ω-slow solutions for quasi-Keplerian rotations.

4.2 Co-existence region between solutions

For a group of eighth different B-type stars (see table 4.7), we studied the region where fast and Ω-slow solutions can co-exist (co-existence region) in two different ways: in the first way not all the stars share the same line-force parameters k and α and in the second one all the stars have the same k and α parameters. For this analysis we only search solutions to models with $0.99 \geq \Omega \geq 0.5$, taking into a count the fact that fast solutions ceases to exist when stars have high rotational rates ($\Omega \gtrsim 0.7$, Curé 2004).

SpT	$T_{\rm eff}$ $[K]$	$log\ g$	$\mathbf{R}_*$ $[R_\odot]$	$\mathbf{M}_*$ $[M_\odot]$	k	α
B0 V	30000	4.0	7.40	17.50	0.571	0.545
B0.5 V	27800	4.0	6.93	15.43	0.571	0.545
B1 V	25400	3.9	6.42	13.21	0.571	0.545
B1.5 V	23000	4.0	5.87	11.04	0.477	0.506
B2 V	20900	3.9	5.33	9.11	0.477	0.506
B3 V	18800	4.0	4.80	7.60	0.477	0.506
B4 V	16800	3.9	4.32	6.62	0.945	0.517
B5 V	15200	4.0	3.90	5.90	0.945	0.517

Table 4.7: Stellar and line-force parameters for differents types of star models. Note that here the B2 V star model is different to the B2 V star model mentioned before.

The stellar parameters of these eight different B-type stars were taken from Arcos et al. (2017) and the line-force parameters were taken from Abbott (1982). Starting with $\gamma_{\rm vis} = 1.0$, we calculated the solutions with HYDWIND to their respective models with different values of Ω. In this first stage, we used freeze ionization ($\delta = 0$). Additionally, we used $\rho_0 = 8.709x10^{-11}\ g\ cm^{-3}$. After that, for each star, we plotted all the terminal velocities (v_∞) and all the mass loss rates ($\dot{M}$) obtained versus the corresponding Ω. Figure 4.8 shows an example of these type of plots, where the interval of Ω values ($\Delta\Omega$) is the called co-existence region. Subsequently, we plotted the value of Ω from the last fast solution found and the value of Ω from the first Ω-slow solution found in the previous step versus $T_{\rm eff}$. We followed the same process for $\gamma_{\rm vis} = 0.95$ and $\gamma_{\rm vis} = 0.90$. Additionally, we calculated fast and Ω-slow solutions, considering that all the stars have the same line-force parameters ($k = 0.587$, $\alpha = 0.530$ and $\delta = 0.0$). Similarly, like above, we plot the value of Ω from the last fast solution found and the value of Ω from the first Ω-slow solution found versus $T_{\rm eff}$ for $\gamma_{\rm vis} = [1.0, 0.95, 0.90]$. Results are represented graphically in figures 4.9 and 4.10.

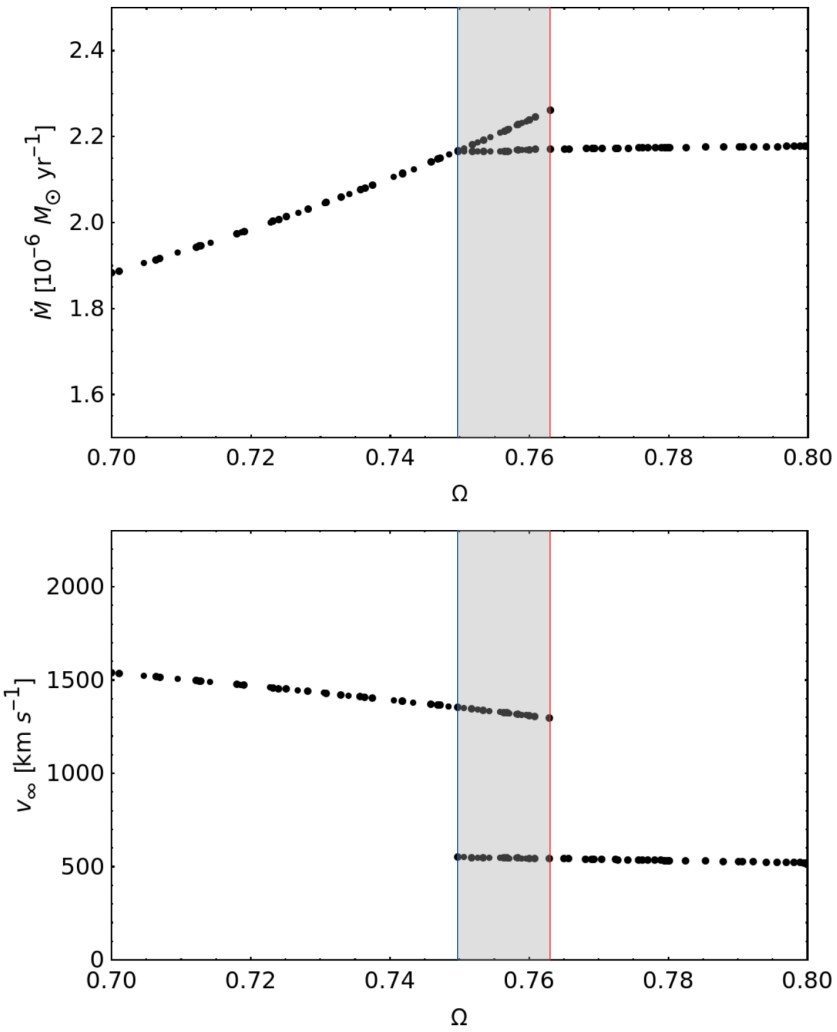

Figure 4.8: Illustrative example of a coexistent region $\Delta\Omega$: $\Delta\Omega$ is represented by the shaded region. The blue line limits the co-existence region when the Ω-slow solutions start and the red line limits the co-existence region when the fast solutions end. This solutions are from the star model B0.5 V; with $\gamma_{\text{vis}} = 0.9$, $k = 0.587$, $\alpha = 0.530$ and $\delta = 0.0$.

In both figures we plot the value of Ω from the last fast solution found and the value of Ω from the first Ω-slow solution found, versus the T_{eff} (respective to each star) for three different values of γ_{vis} (1.0, 0.95 and 0.90). In other words, we translate the range of values of Ω (X axis) of the co-existence regions obtained for each star (see plot 4.8) and then we place them on the Y axis of the figures 4.9 and 4.10, depending on T_{eff}. The results were the same for both plots: when γ_{vis} decreases or when α increases, the range of Ω values are shifted to higher Ω values. Furthermore, this changes do not depend neither of the T_{eff} nor k.

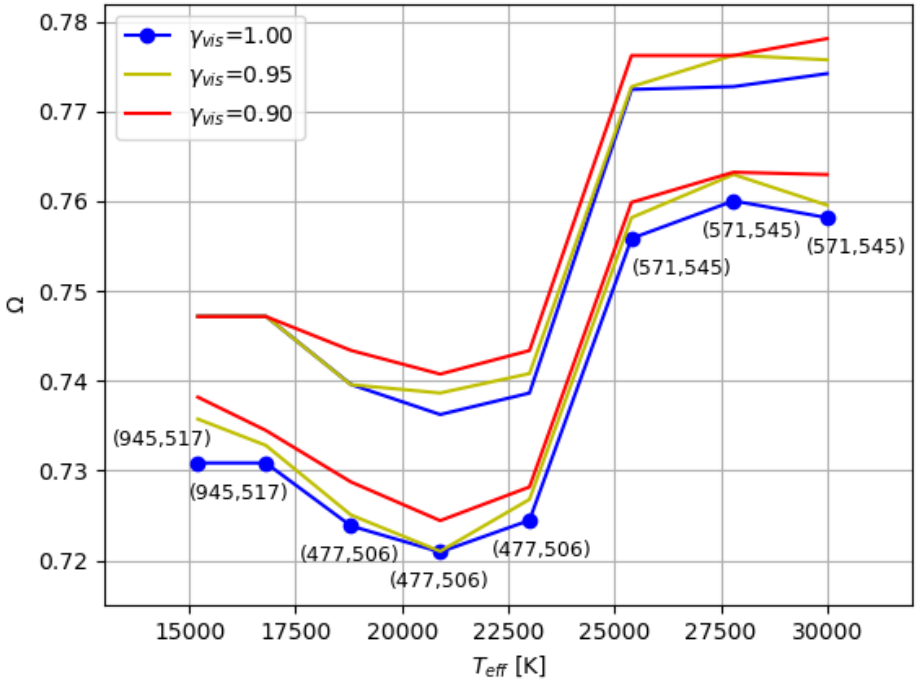

Figure 4.9: Co-existence regions for each Be star model. The points in blue only represent the values of (k,α) used, multiplied by 1000. When $\gamma_{\rm vis}$ decreases or when α increases, the range of Ω values belonging to co-existence region are shifted to higher Ω values.

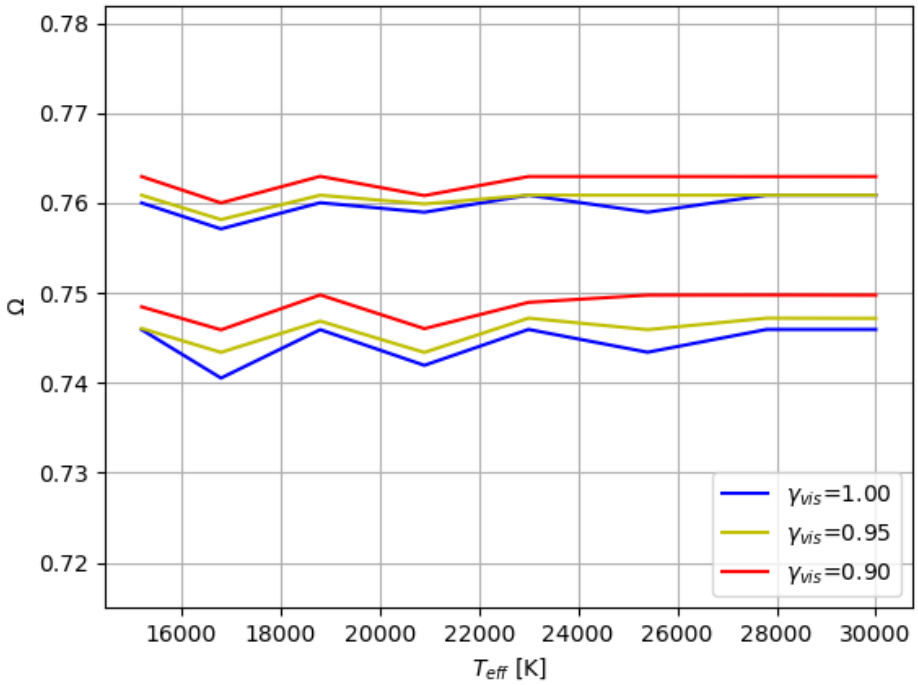

Figure 4.10: Co-existence regions for each Be star model, considering that all the stars have the same line-force parameters. The result is the same that the result of the figure above.

4.2.1 The δ-GAP

When a star with values of Ω in an interval of $0.99 \geq \Omega \geq 0.5$ is modeled, the aforementioned region of co-existence can be found. But, in what cases does this region not exist or cease to exist? Previously, Araya et al. (2018) studied this phenomenon for a B2.5 V star, considering $\gamma_{\rm vis} = 1.0$. In their work, the region of co-existence ceased to exist when $\delta > 0.4$, forming a gap (similar to figure 4.11) called δ-GAP.

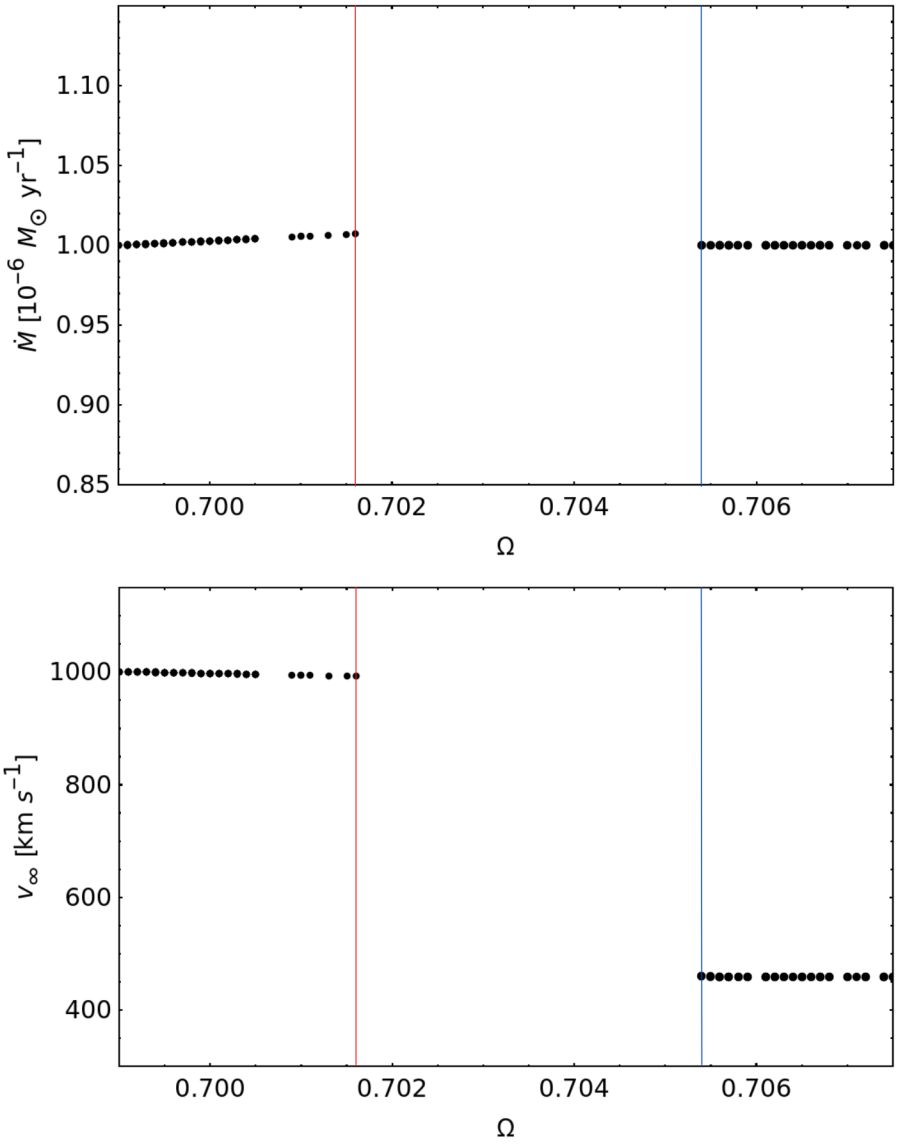

Figure 4.11: Illustrative example of a $\delta - GAP$: here there are not a region of co-existence. The blue line limits the co-existence region when the Ω-slow solutions start and the red line limits the co-existence region when the fast solutions end. This solutions are from the star model B2 V; with $\gamma_{\rm vis} = 0.95$, $k = 0.587$, $\alpha = 0.530$ and $\delta = 0.04$.

To know the influence of γ_{vis} in the co-existence region when we study the ionization changes (given by δ), we use $k = 0.587$ and $\alpha = 0.530$, and vary the value of δ from 0.01 to 0.05 for all the stars in table 4.7. We only use $\gamma_{\text{vis}} = 1.0$ and $\gamma_{\text{vis}} = 0.95$. As a first instance, the co-existence regions appear to be shifted towards larger values of Ω. However, γ_{vis} does not appear to affect the wide of the co-existence region, as does δ. Additionally, co-existence region cease to exist for $\delta > 0.03$ (we omit these values in the tables below).

SpT	**co-existence Region with $\gamma_{\text{vis}} = 1.00$**		
	$\delta = 0.01$	$\delta = 0.02$	$\delta = 0.03$
B0 V	$0.739 < \Omega < 0.747$	$0.726 < \Omega < 0.733$	$0.716 < \Omega < 0.719$
B0.5 V	$0.740 < \Omega < 0.746$	$0.727 < \Omega < 0.732$	$0.717 < \Omega < 0.718$
B1 V	$0.741 < \Omega < 0.746$	$0.723 < \Omega < 0.731$	$0.7164 < \Omega < 0.7172$
B1.5 V	$0.737 < \Omega < 0.746$	$0.731 < \Omega < 0.732$	$0.7168 < \Omega < 0.7170$
B2 V	$0.733 < \Omega < 0.744$	$0.724 < \Omega < 0.729$	$0.713 < \Omega < 0.714$
B3 V	$0.747 < \Omega < 0.746$	$0.731 < \Omega < 0.731$	$0.7161 < \Omega < 0.7164$
B4 V	$0.732 < \Omega < 0.743$	$0.722 < \Omega < 0.728$	$0.712 < \Omega < 0.713$
B5 V	$0.745 < \Omega < 0.745$	$0.726 < \Omega < 0.729$	$0.7144 < \Omega < 0.7153$

Table 4.8: Intervals of Ω where fast and Ω-slow solutions co-exist, considering $\gamma_{\text{vis}} = 1.00$.

SpT	**co-existence Region with $\gamma_{\text{vis}} = 0.95$**		
	$\delta = 0.01$	$\delta = 0.02$	$\delta = 0.03$
B0 V	$0.739 < \Omega < 0.749$	$0.729 < \Omega < 0.734$	$0.719 < \Omega < 0.720$
B0.5 V	$0.749 < \Omega < 0.750$	$0.729 < \Omega < 0.734$	$0.7193 < \Omega < 0.7195$
B1 V	$0.742 < \Omega < 0.747$	$0.727 < \Omega < 0.733$	$0.717 < \Omega < 0.718$
B1.5 V	$0.739 < \Omega < 0.748$	$0.729 < \Omega < 0.733$	$0.7177 < \Omega < 0.7182$
B2 V	$0.734 < \Omega < 0.746$	$0.724 < \Omega < 0.731$	$0.716 < \Omega < 0.717$
B3 V	$0.737 < \Omega < 0.747$	$0.728 < \Omega < 0.733$	$0.7178 < \Omega < 0.7184$
B4 V	$0.734 < \Omega < 0.747$	$0.724 < \Omega < 0.730$	$0.714 < \Omega < 0.715$
B5 V	$0.737 < \Omega < 0.747$	$0.726 < \Omega < 0.731$	$0.717 < \Omega < 0.718$

Table 4.9: Intervals of Ω where fast and Ω-slow solutions co-exist, considering $\gamma_{\text{vis}} = 0.95$.

Later, in order to study the behavior of fast and Ω-slow solutions in δ-GAP, we also

used results of HYDWIND in the ZEUS calculations.These HYDWIND results were used as an initial guess on the calculations of ZEUS at the edges of the δ-GAPs, beginning from the last fast solution to the first Ω-slow solution or from the first Ω-slow solution to the last fast solution (depending of the edge studied), going in small intervals of Ω. We also tried to use the last result calculated with ZEUS as an initial guess on the next calculation, and so on. For both cases, the solution did not converge to a stationary solution, no matter what the trial velocity profile we used.

CHAPTER 5

Discussion

In the hydrodynamic analysis of the winds from very fast rotating stars, such as Be stars, the implementation of stellar rotation in the equation of motion of radiation driven winds is essential. We model this rotation by means of the parameter $\Omega = v_{rot}/v_{crit}$ (see chapter 2 for details). On the other hand, the wind of a rotating star also rotates and the way it does depends on different physical phenomena: whether or not there are torques in the wind, such as those caused by the presence of viscosity, and/or whether or not the star has strong magnetic fields.

Since we want to model rotating winds without conserving angular momentum, on the basis that a torque provided by a viscous shear can change the angular momentum of a rotating object, we add a simulated viscosity parameter (referred to in this work as $\gamma_{\rm vis}$) to the 1D stationary EoM in the equatorial plane for radiation driven winds. Thus when $\gamma_{\rm vis} = 1$ the wind rotates conserving angular momentum, i.e, the azimuthal velocity of the wind (v_ϕ) falls as the inverse of the distance to the star. On the other hand, as a consequence of the angular momentum transport along the wind due to the presence of viscosity, when $\gamma_{\rm vis} = 0.5$ the wind rotates in a Keplerian way, i.e, the angular momentum of the wind grows with radius as $r^{-1/2}$. In this way, material that is ejected at the stellar photosphere must have its angular momentum doubled in order to reach an orbit of $4R_*$ (Rivinius et al. 2013). The model that offers an explanation for this phenomenon is the viscous decretion

disk model of Lee et al. (1991), knowing as VDD (Rivinius et al. 2013, Curé et al. 2022).

In order to study the behavior of fast and Ω-slow solutions by implementing $\gamma_{\rm vis}$ to the EoM and varying the line force parameters, we use different values of k, α and δ. In other words, in this work we study the rotation of the drecretion-disk of Be stars by varying the relative importance of the thin and thick lines with the parameter α, by varying the changes in ionization along the wind with the parameter δ and by varying the total number of contributing lines with the parameter k.

For our models we take into account values of δ in the range $0.00 \leq \delta \leq 0.05$, considering that when $\delta \simeq 0$, the changes in ionization along the wind are negligible. On the other hand, we use different values of α, considering that while the thick lines do not contribute when $\alpha = 0$, the opposite happens when $\alpha = 1$. However, because we had numerical difficulties in obtaining solutions when considering values of $\alpha \leq 0.4$ (similar to de Araujo et al. 1994), we limit ourselves to using values of α greater than 0.4. Additionally, although we use different values of k, this parameter hardly affects the results and its variation can be neglected.

Let us remember that our models are theoretical and, furthermore, they have computational limitations that restrict the values of the line force parameters involved to being only test values without associated uncertainties. It is expected that in future works uncertainties may be associated with the results. However, even with more precise theoretical models, it should be kept in mind that measuring the terminal wind speed v_∞ is very complicated, since the edge of the line profiles is not clear and v_∞ might not be well represented (Snow 1981).

5.1 B2.5 V star model

Until 1994, the main drawback of the theoretical models was that compared to the observational results, they produced a strong equatorial expansion ($v_\infty \geq 1000\ km/s$). One of the examples of these observational results are those obtained by Poeckert & Marlborough (1978), where the best fit of the profile of the Hα line of the Be star γ Cas (B0.5 IV) was obtained when the terminal velocity at 40 $R_\star$ was equal to 200 km/s. Another study of the star γ Cas was done by Stee et al. (1995), where they found that a terminal velocity of 400 km/s produced a line profile excessively broadened and a

terminal velocity of 100 km/s produced a very narrow line, compared to the profile observed from interferometric measurements of the Hα line. On average the terminal velocity that best fit was $\sim$200 km/s (150 $km/s \geq v_\infty \geq 250\ km/s$). Another of these examples is that of the Be star α Ara (B3 V), which by adjusting the profiles of the lines of Hα, Hβ and Paβ, obtains a terminal velocity of $170 \pm 20\ km/s$ at 22 $R_\star$ (Chesneau et al. 2005).

As a consequence, over the last few decades it has been attempted to find theoretical terminal wind speeds of around $200\,km/s$. For example, Stee et al. (1995) searched for an equatorial hydrodynamic solution for the star γ Cas that fit their observational results ($v_\infty \sim 200\,km/s$) and found that the line force parameters $\alpha = 0.05$ and $k = 10.5$ produced a terminal velocity of 201 km/s at 100 $R_\star$. In other words, to obtain very low winds terminal velocities in the equatorial plane, it was necessary to consider that the wind is largely driven by thin lines, as de Araujo (1995) concluded.

For the B2.5 V type star that we studied, we find a lowest terminal velocity ($v_\infty \sim 112\,km/s$) in a Ω-slow solution, considering that: (1) the star has a very high rotation ($\Omega = 0.99$), (2) the changes in ionization along the wind are negligible ($\delta \simeq 0$), (3) the wind is driven by slightly more optically thin lines than thick lines ($\alpha = 0.45$) and (4) the wind rotates in a quasi-Keplerian way ($\gamma_{\rm vis} = 0.5103$).

The decretion-disks of Be stars are known to possess a Keplerian velocity field (see for example Meilland et al. 2007, Delaa et al. 2011, Kraus et al. 2012). Thus if we consider that decretion-disks are winds transported radially and rotating in a Keplerian way ($\gamma_{\rm vis} = 0.5$), our result ($\gamma_{\rm vis} \sim 0.5$) is consistent with the observations, although our work is developed only in the equatorial plane. However, probably because we did not consider oblateness and GD effects, this solution has an initial velocity in the star's photosphere close to the isothermal sound speed. Time-dependent hydrodynamical code ZEUS helped us to corroborate that this result was not just an error of HYDWIND.

On the other hand, by varying the values of $\gamma_{\rm vis}$, in the range $0.5 \lesssim \gamma_{\rm vis} \leq 1.0$, and the values of Ω, in the range $0.50 \leq \Omega \leq 0.99$, and leaving the other stellar parameters and the line force parameters fixed, we study which solutions to the stationary equation of motion are found (fast or Ω-slow solutions) when the wind rotates in a

quasi-Kleplerian way. For our B2.5 V type star, we find that the fast solutions have a different behaviour than the Ω-slow solutions (see figure 4.5). In the case of fast solutions, winds have higher terminal velocities as $\gamma_{\rm vis} \longrightarrow 1.0$. With the Ω-slow solutions the opposite happens: terminal velocities decreases when $\gamma_{vis} \longrightarrow 1.0$.

Additionally, topologically, when the wind rotates in a quasi-Keplerian way, the plane $F(u, Z) = 0$ intersects the function $F(u, Z)$ at a greater number of points (see appendix A). In other words, when the wind rotates in a quasi-Keplerian way, the probability of obtaining an Ω-slow solution decreases. This effect can also be seen in figure 4.7.

5.2 The co-existence region

As mentioned previously, based on the work done by Araya et al. (2018), we consider eight different B V-type stars and study the region where fast solutions can co-exist alongside Ω-slow solutions, i.e., the called co-existence region. In other words, the co-existence region is the interval of values of Ω (ΔΩ) from the plots of v_∞ versus Ω and/or $\dot{M}$ versus Ω, where both types of solutions are found simultaneously.

In this way, for each type of star (according to its $T_{\rm eff}$), the ends of the interval ΔΩ can be extracted from the plots v_∞ versus Ω and/or $\dot{M}$ versus Ω, and then, plot this values of Ω as function of $T_{\rm eff}$. Doing that it is possible to analyze the influence of line-force parameters and the influence of $\gamma_{\rm vis}$ in the co-existence region when the stellar parameters change. In other words, with plots of Ω versus $T_{\rm eff}$, we analyze what are the conditions for a Be star to form or dissipate a drecretion-disk; knowing that the co-existence region could be related to the creation and/or dissipation of drecretion-disks in Be stars when the base of the wind is disturbed (Araya et al. 2018).

For this part of our investigation, based on Abbott (1982) and Arcos et al. (2017), we first consider average values of α and k, where the same for all stars. Subsequently, we assign different values of α and k for each star. By presenting a region of co-existence, the results indicate that all the stars studied here are capable of forming and/or dissipating a drecretion-disk when the wind rotates close to the conservation of angular momentum ($0.9 \leq \gamma_{\rm vis} \leq 1.0$). Additionally, the results show that values of $\gamma_{\rm vis} < 1.0$ shift ΔΩ to larger values of Ω, which means that when the wind rotates in

a quasi-Keplerian way, the formation and/or dissipation of the drecretion-disk could be triggered in very fast rotating stars. Similarly, it is confirmed that $\Delta\Omega$ region also shifts towards higher values of Ω when α increases its value and that $\Delta\Omega$ decreases its wide when we slightly increase the value of δ, as mentioned by Araya et al. (2018). So far, there are three possibilities for the drecretion-disk to develop in very fast-rotating stars: when the drecretion-disk rotates in a quasi-Kleplerian way, when thin lines contribute slightly more to the radiation force than thick lines, or a combination of both processes.

The co-existence region can disappear and form a gap between the fast solutions and the Ω-slow solutions if changes in ionization along the wind become relevant ($\delta > 0.03$). For this reason, we called δ-GAP to this gap. Similarly, we find that the co-existence region shows anomalies (kinks in the velocity profiles) in some stars and simply does not show up in others when the wind rotation approaches the Keplerian rotation. We corroborated this last result using ZEUS, since this time-dependent code converges in time to a stationary solution. From the work of Araya et al. (2018), we knew that these type of anomalies are caused by the type of solution that is used as a test solution in the calculation of the computational model.

CHAPTER 6

Conclusions

From the study of the behaviour of wind solutions (fast and Ω-slow), considering models with winds rotating in a quasi-Keplerian way, the main aim of this work was to obtain a wind velocity profile that adequately describes the decretion-disk of classical Be stars, i.e., to find theoretical models without angular momentum conservation that can reproduce the observational results.

Here we found the lowest terminal velocities in Ω-slow solutions, when the star rotates close to its critical velocity, and when its wind rotates in a quasi-Keplerian way, very close to the Keplerian rotation: In the case of the B2 V star model, considering $\Omega = 0.99$ and $\gamma_{\rm vis} = 0.52$, the terminal velocity of the wind was $v_\infty \sim 106\, km/s$. For the B2.5 V star model the terminal velocity of the wind has its minimum when the model has $\Omega = 0.99$ and a $\gamma_{\rm vis} = 0.5103$. Thus the lowest wind terminal velocity founded for this model was $v_\infty \sim 112\, km/s$. Therefore, we conclude that $\gamma_{\rm vis}$ slow downs terminal velocity of the winds of classical Be stars.

Although we did not reproduce the line profiles to compare our results with spectral observations, from Ω-slow solutions, we obtain velocity profiles that reproduce good the terminal velocity of the observational results of Be stars previously done by other authors, whose decretion-disks have terminal velocities of less than $250\, km/s$ (Poeckert & Marlborough 1978, Chesneau et al. 2005, Rivinius et al. 2013).

On the other hand, considering that there is no change in ionization along the wind ($\delta = 0$), all the stars in our sample of eight different main sequence B-type stars presented what we call a co-existence region, which is possibly related to the mechanism that forms and/or dissipates the decretion-disk that characterizes Be stars (Araya et al. 2018). In turn, for all the eight stars, the interval of values of Ω ($\Delta\Omega$) corresponding to the co-existence region shifts towards higher values of Ω when $\gamma_{\rm vis}$ decreases (i.e., when the wind rotates in a quasi-Keplerian way) and when α increases (i.e., when the wind is driven by more optically thick lines than optically thin lines). In conclusion: (1) co-existence region exists for the entire range of temperatures $T = (15000, 30000)\ K$ and (2) the lower is $\gamma_{\rm vis}$ the higher is the shift of $\Delta\Omega$.

Additionally, $\Delta\Omega$ is reduced when the value of δ increase slightly. That is, for $\delta > 0.03$ the co-existence region disappears and a gap (called δ-GAP) is formed, which increases in size as δ increases in value. Finally, due to we only analyze the δ-GAP with the stationary code HYDWIND, we conclude that the δ-GAP needs to be studied with time-dependent codes in order to obtain results more precise.

We confirm that Ω-slow solutions could reproduce the observational results when the wind rotates in a quasi-Keplerian way. Because of this, our findings could strongly contribute in the explanation of the disk formation and/or dissipation mechanism in Be stars if in the future the oblate form of stars with high rotation is considered and if the parameters of the line-force are calculated in a self-consistent way.

6.1 Future work

Some solutions of the B2.5 V model, including the one with the lowest terminal velocity, had velocities in the photosphere close to the isothermal speed of sound. This is not physically acceptable because it means that the wind speed is almost sonic at the base of the wind and therefore, the sonic point would be very close to the photosphere.

Since the star begin to change their spherical shape as their rotational speed increases, and thus the effective temperature varies as a function of stellar latitude, when stars rotate very fast ($\Omega \gtrsim 0.7$) it becomes necessary consider the oblate shape that stars adopt and the GD effect (section 2.1.1). Due to this, in next works we will

consider this effects to corroborate that the change in the equatorial radius of the B2.5 V model gives consistent results.

On the other hand, in order to give more complete conclusions, it is intended to continue studying the co-existence region of the B-type stars already considered in this work for $0.5 < \gamma_{\rm vis} < 0.9$. Additionally, an analysis in more than one dimension could give more accurate answers regarding the region of co-existence. Also we would like to implement line-force parameters obtained in an self-consistent way to work with the most adequate line-force parameters according to the stellar parameters.

In order to obtain solutions that can better fit the observations, in future models with winds rotating in a quasi-Keplerian way, it is expected to apply all the previously mentioned objectives to the equatorial models developed in this work. After that, we intend to use the radiative transfer code HDUST (Carciofi & Bjorkman 2006) to obtain the theoretical spectrum of the Hα line and then compares our results with the observations.

Appendix A

Location of the critical point

In order that the theory can correctly reproduce the observational results of terminal velocity and mass loss rate, the solution of the equation of motion (EoM) for radiation driven isothermal stellar winds must have a velocity law that starts with a small value at the stellar surface and reach supersonic speeds far away from the star, passing through a singular point. This occurs at the so-called, critical point, where the partial derivative of the function F_A, equation 2.20, with respect to w' becomes zero (*singularity condition*: see equation A.1 below). For more details about singularity condition see for example Lamers & Cassinelli (1999), Cassinelli (1979), Curé (2004), Curé & Rial (2007). Thus,

$$\frac{\partial F_A}{\partial w'} = \left(1 - \frac{1}{w^2}\right) w - C' \left(\frac{\partial CF}{\partial w'} + \alpha \frac{CF}{w'}\right) g w^{-\delta} (w w')^{\alpha} = 0. \tag{A.1}$$

Also, since $F_A = 0$, a *regularity condition* must be imposed at the critical point:

$$\frac{dF_A}{du} = \frac{\partial F_A}{\partial u} + \frac{\partial F_A}{\partial w} w' = 0. \tag{A.2}$$

$$\frac{\partial F_A}{\partial u} = -C' \left(g \frac{\partial CF}{\partial u} + CF \frac{\partial g}{\partial u}\right) w^{-\delta} (w w')^{\alpha} - \frac{2}{u^2} + a_{rot}^2 \mathbf{(2\gamma_{vis} - 1)(-u)^{2\gamma_{vis} - 2}}. \tag{A.3}$$

$$\frac{\partial F_A}{\partial w} = \left(1 + \frac{1}{w^2}\right) w' - C' \left(\frac{\partial CF}{\partial w} + \alpha \frac{CF}{w} - \delta \frac{CF}{w}\right) g w^{-\delta} (w w')^{\alpha}. \tag{A.4}$$

A.1 Critical point functions

To complement the search of solutions to the EoM of radiation driven winds and considering the possible effects of $\gamma_{\rm vis}$ on the topology of the solutions, we recalculate the functions $R(u,Z)$ and $H(u,Z,C')$ (Curé (2004); Curé & Rial (2007)) from equation 2.20.

A.1.1 Coordinates transformation

Based on Curé (2004), with $Y = ww'$ and $Z = w/w'$, equation 2.20 becomes:

$$\left(1-\frac{1}{YZ}\right)Y+\frac{2}{u}+A\left[1-\boldsymbol{\Omega^2(-u)^{2\gamma_{\rm vis}-1}}\right]-C'f_1(u,Z)\,g(u)\,Z^{-\delta/2}\,Y^{\alpha-\delta/2}=0, \tag{A.5}$$

where $f_1(u,Z) = CF(u,Z)$.

As the same way, singularity condition A.1 becomes into

$$\left(1-\frac{1}{YZ}\right)Y-C'f_2(u,Z)\,g(u)\,Z^{-\delta/2}\,Y^{\alpha-\delta/2}=0 \tag{A.6}$$

And

$$C'=\frac{1}{g(u)\,f_2}\left(1-\frac{1}{YZ}\right)Z^{\delta/2}\,Y^{1-\alpha+\delta/2}, \tag{A.7}$$

where $f_2(u,Z) = \alpha f_1(u,Z) + uZe(u,Z)$ and $e(u,Z) \equiv -\frac{w'}{uZ}\frac{\partial CF}{\partial w'}$.

Thus, then regularity condition A.2 becomes into

$$\begin{aligned}\left(1-\tfrac{1}{YZ}\right)Y-\tfrac{2Z}{u^2}+a_{rot}^2\boldsymbol{(2\gamma_{\rm vis}-1)(-u)^{2\gamma_{\rm vis}-2}}\,Z\\ -C'f_3(u,Z)\,g(u)\,Z^{-\delta/2}\,Y^{\alpha-\delta/2}=0,\end{aligned} \tag{A.8}$$

with $f_3(u,Z) = (3u+Z)Ze(u,Z) + f_1(u,Z)\,[h(u)Z+\alpha-\delta]$ and $h(u) \equiv \frac{1}{g(u)}\frac{dg(u)}{du}$.

Now, substracting equation A.5 to equation A.6, we obtain

$$C'g(u)\,Z^{-\delta/2}\,Y^{\alpha-\delta/2}=\frac{1}{f_1-f_2}\left[\frac{2}{u}+A-\boldsymbol{a_{rot}^2(-u)^{2\gamma_{\rm vis}-1}}\right]. \tag{A.9}$$

Finally, substituting equation A.9 in equation A.6 the expression turns into

$$Y = \frac{1}{Z} + \frac{f_2}{f_1 - f_2}\left[\frac{2}{u} + A - \boldsymbol{a_{rot}^2}(-\boldsymbol{u})^{\mathbf{2\gamma_{vis}-1}}\right]. \tag{A.10}$$

A.1.2 The critical point of function R(u,Z)

The function $R(u, Z)$ was derived by Curé (2004) through a coordinates transformation in the EoM, in the singularity condition and in the regularity condition. This function depends only of two variables, which makes it possible to plot it in 3D and find the location of the roots of the function, it is at the intersection with the plane $R(u, Z) = 0$. In this way, after knowing the range of Z values, where the function is defined, and considering the initial conditions of the EoM, a root is found that corresponds to the critical point u_{crit}, that will give rise to the only numerical solution of the momentum equation. This procedure led to Curé (2004) to discover a new family of solutions: the Ω-slow solutions.

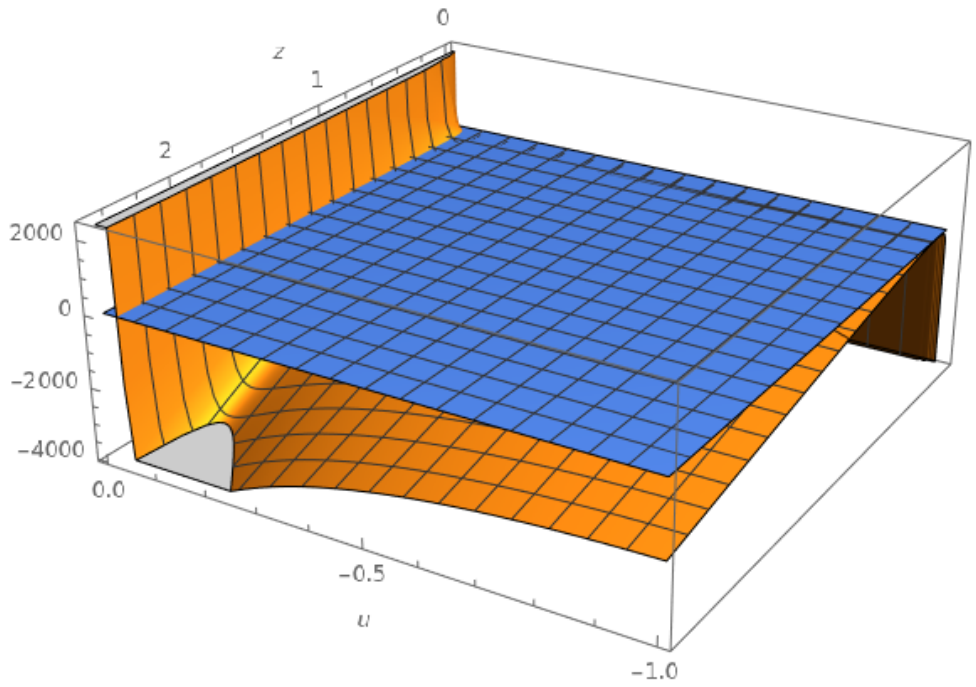

Figure A.1: Topology of solutions for a model with $T_{eff} = 20000$ K, $R_* = 4.0$ $R_\odot$, $log\ g = 4.11$, $Z_{He} = 1.0$, $k = 0.61$, $\alpha = 0.45$, $\delta = 0.0$, $\Omega = 0.9$ and $\gamma_{\rm vis} = 0.9$. Blue surface is the plane $R(u, Z) = 0$ and orange surface is $R(u, Z)$ function. The intersection of both surfaces close to $u = 0.0$ correspond to the family of Ω-slow solutions. See Curé (2004) for more details about the topology of solutions.

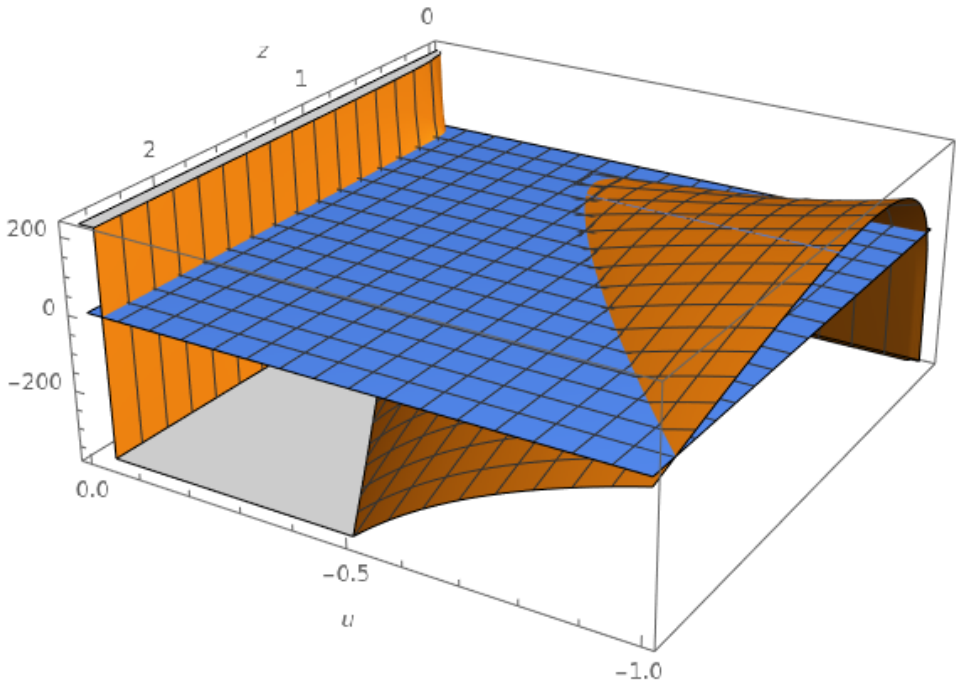

Figure A.2: In comparison with figure A.1, this model has $\gamma_{\rm vis} = 0.53$. A displacement of the function $R(u, Z)$ to positive values is observed. This displacement gives rise to another intersection of plane $R(u, Z) = 0$ and $R(u, Z)$ function, that is the family of fast solutions.

To analyze the topology of both families of solutions, fast solutions and Ω-slow solutions, in a quasi-Keplerian wind ($0.5 < \gamma_{\rm vis} < 1$), we recalculate the function $R(u, Z)$. Thus, subtracting equation A.8 to equation A.6 and substituting equation A.9, we get:

$$\begin{aligned} R(u,Z) \equiv & -\frac{2}{Z} + \frac{2Z}{u^2} - a_{rot}^2 \mathbf{(2\gamma_{vis} - 1)(-u)^{2\gamma_{vis}-2}}\, Z \\ & + f_{123}\left[\frac{2}{u} + A - \boldsymbol{a_{rot}^2(-u)^{2\gamma_{vis}-1}}\right], \end{aligned} \tag{A.11}$$

where $f_{123} = \frac{(f_2 - f_3)}{(f_2 - f_1)}$.

A.1.3 The critical point function H(u,Z,C')

Another function that is also used to locate critical points for a given eigenvalue is the $H(u, Z, C')$ function. Substracting C' to both sides of the equality in equation A.7 and

substituting equation A.10 in equation A.7, $H(u, Z, C')$ is expressed as

$$H(u,Z,C') \equiv -C' + \frac{1}{g(u)\,(f_1 - f_2)}\left[\frac{2}{u} + A - \boldsymbol{a_{rot}^2(-u)^{2\gamma_{vis}-1}}\right] \left\{Z^{\alpha-1} + \frac{f_2}{f_1 - f_2}\left[\frac{2}{u} + A - \boldsymbol{a_{rot}^2(-u)^{2\gamma_{vis}-1}}\right] Z^{\alpha}\right\}^{\delta/2-\alpha}. \quad \text{(A.12)}$$

As critical points are found graphically at the intersection of the function $R(u, Z)$ with the plane $R(u, Z) = 0$, in a certain range of Z, critical points can also be found in a 2D-plot at the intersection of the function $R(u, Z)$ with the function $H(u, Z, C')$ (considering a value of C' appropriate to the model in question). In this way, the number of possible critical points to resolve the EoM is considerably reduced using the both functions, since the points where these planes intersect are potential critical points. However, as Curé & Rial (2007) mention, the number of those critical points depends on the value of C'.

Using the previous graphical methods an approximation of the position of the critical points of the models with winds rotating in a quasi-Keplerian way can be given, and with this, the solutions to the EoM, that can be compared with the numerical solutions obtained with the hydrodynamic code HYDWIND.

Bibliography

Abbott D. C., 1982, ApJ, 259, 282

Araya I., Curé M., 2020, User Guide for HYDWIND, Universidad Mayor & Universidad de Valparaíso

Araya I., Curé M., ud Doula A., Santillán A., Cidale L., 2018, Monthly Notices of the Royal Astronomical Society, 477, 755–765

Arcos C., Jones C. E., Sigut T. A. A., Kanaan S., Curé M., 2017, ApJ, 842, 48

Bjorkman J. E., Cassinelli J. P., 1993, ApJ, 409, 429

Carciofi A. C., Bjorkman J. E., 2006, ApJ, 639, 1081

Cassinelli J. P., 1979, ARA&A, 17, 275

Castor J. I., Abbott D. C., Klein R. I., 1975, ApJ, 195, 157

Castor J. L., 1974, MNRAS, 169, 279

Chesneau O. et al., 2005, A&A, 435, 275

Clarke D. A., 1996, ApJ, 457, 291

Cochetti Y. R., Zorec J., Cidale L. S., Arias M. L., Aidelman Y., Torres A. F., Frémat Y., Granada A., 2020, A&A, 634, A18

Cranmer S. R., Owocki S. P., 1995, ApJ, 440, 308

Curé M., Meneses R., Araya I., Arcos C., Peña G., Machuca N., Rodriguez A., 2022, arXiv e-prints, arXiv:2206.09031

Curé M., 2004, The Astrophysical Journal, 614, 929–941

Curé M., Rial D. F., 2007, Astronomische Nachrichten, 328, 513–520

de Araujo F. X., 1995, A&A, 298, 179

de Araujo F. X., de Freitas Pacheco J. A., Petrini D., 1994, MNRAS, 267, 501

Delaa O. et al., 2011, A&A, 529, A87

Espinosa Lara F., Rieutord M., 2011, A&A, 533, A43

Friend D. B., Abbott D. C., 1986, ApJ, 311, 701

Gayley K. G., 1995, ApJ, 454, 410

Gormaz-Matamala A. C., Curé M., Cidale L. S., Venero R. O. J., 2019, ApJ, 873, 131

Gray D. F., 2005, The Observation and Analysis of Stellar Photospheres

Kasai E., 2013, Ph.D. thesis

Kogure T., Leung K.-C., 2007, The Astrophysics of Emission-Line Stars, Vol. 342

Kraus S. et al., 2012, ApJ, 744, 19

Lamers H. J. G., Pauldrach A. W. A., 1991, A&A, 244, L5

Lamers H. J. G. L. M., Cassinelli J. P., 1999, Introduction to Stellar Winds

Lee U., Osaki Y., Saio H., 1991, MNRAS, 250, 432

Lucy L. B., Solomon P. M., 1970, ApJ, 159, 879

Maeder A., 2009, Physics, Formation and Evolution of Rotating Stars

Meilland A. et al., 2007, A&A, 464, 59

Morton D. C., 1967, ApJ, 147, 1017

Parker E. N., 1958, ApJ, 128, 664

Parker E. N., 1960, ApJ, 132, 821

Pauldrach A., Puls J., Kudritzki R. P., 1986, A&A, 164, 86

Poeckert R., Marlborough J. M., 1978, ApJ, 220, 940

Rivinius T., Carciofi A. C., Martayan C., 2013, A&A Rev., 21, 69

Snow J., T. P., 1981, ApJ, 251, 139

Snow J., T. P., Morton D. C., 1976, ApJS, 32, 429

Stee P., de Araujo F., 1994, Symposium - International Astronomical Union, 162, 470–472

Stee P., de Araujo F. X., Vakili F., Mourard D., Arnold L., Bonneau D., Morand F., Tallon-Bosc I., 1995, A&A, 300, 219

Venero R. O. J., Curé M., Cidale L. S., Araya I., 2016, ApJ, 822, 28

von Zeipel H., 1924, MNRAS, 84, 684